2020-12-09

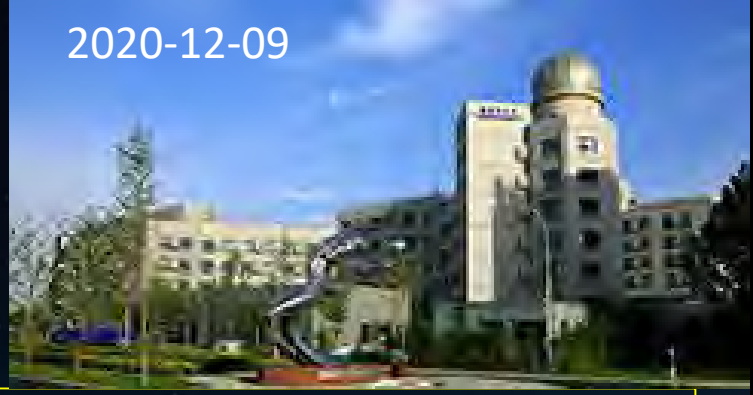

Direct Observations of Fast Inflow Directly Feeding Quasar Accretion Disks

by HI* & HeI*

中国科学技术大学
中国极地研究中心

南极天文学研究室 周宏岩 *in cooperation with*

史习珩，袁为民，郝蕾，陈向军，葛健，纪拓，姜鹏，李歌，刘碧芳，刘桂琳，刘文娟，陆红琳，潘翔，沈俊太，舒新文，孙鹿鸣，田启国，王慧元，王挺贵，吴胜杏，杨臣威，张少华，钟邳浩

Outline

1. what/why black holes?
2. why massive black hole inflow?
3. how to track accretion flows?
   a: **HI*** & **HeI*** absorption lines
4. a case study (J1035+1422): disk-feeding-inflow
5. **analogues**: head and end of disk-feeding-inflow
6. what next (jet vs. outflow)?

GRAVITATIONAL COLLAPSE AND SPACE-TIME SINGULARITIES

Roger Penrose
Department of Mathematics, Birkbeck College, London, England
(Received 18 December 1964)

The discovery of the quasistellar radio sources has stimulated renewed interest in the question of gravitational collapse. It has been suggested by some authors[1] that the enormous amounts of energy that these objects apparently emit may result from the collapse of a mass of the order of $(10^8\text{-}10^9)M_\odot$ to the neighborhood of its Schwarzschild radius, accompanied by a violent release of energy, possibly in the form of gravitational radiation. The detailed mathematical discussion of such situations is difficult since the full complexity of general relativity is required. Consequently, most exact calculations concerned with the implications of gravitational collapse have employed the simplifying assumption of spherical symmetry. Unfortunately, this precludes any detailed discussion of gravitational radiation – which requires at least a quadripole structure.

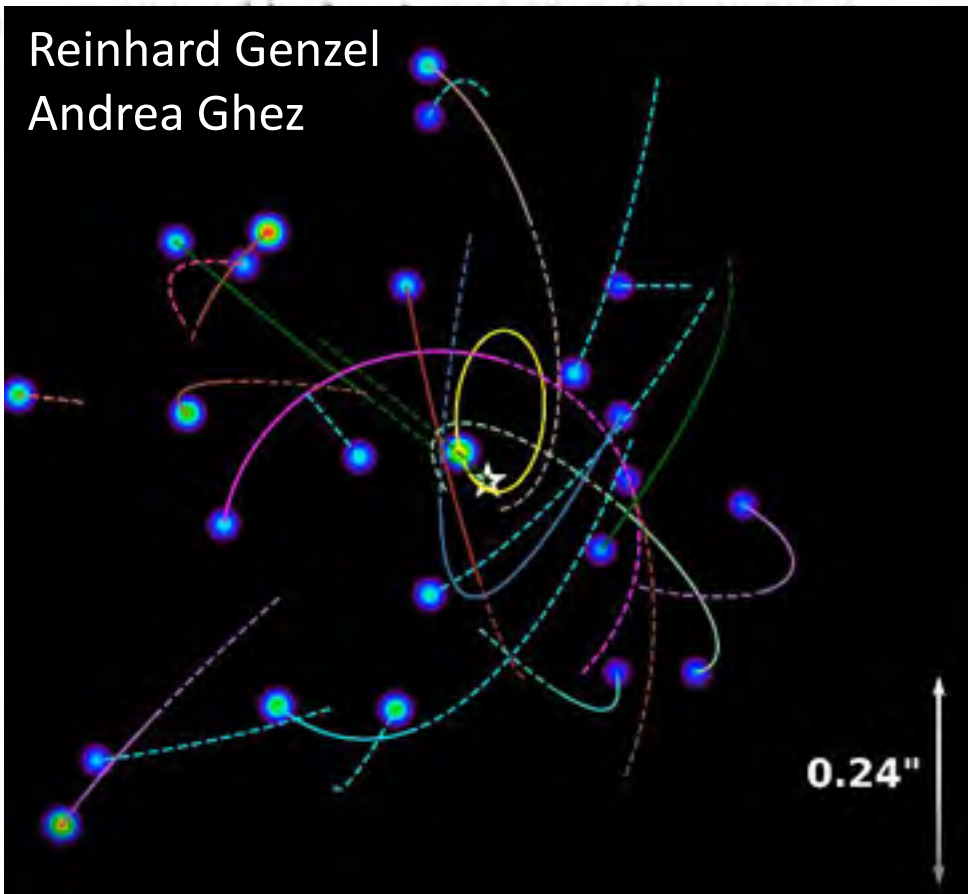

1. what/why black holes?

(1) primeval; (2) stellar, (3) (super-)massive black holes

1. What are black holes?

- 尸佼:“四方上下曰宇，往古今来曰宙”
- **Einstein: geometrodynamics**
  physical para. & law

- events: “points” in space-time
- Riemannian geometry
- Einstein’s Eq.
- Hawking-Penrose’s singularity theorems:
- black holes and the big bang

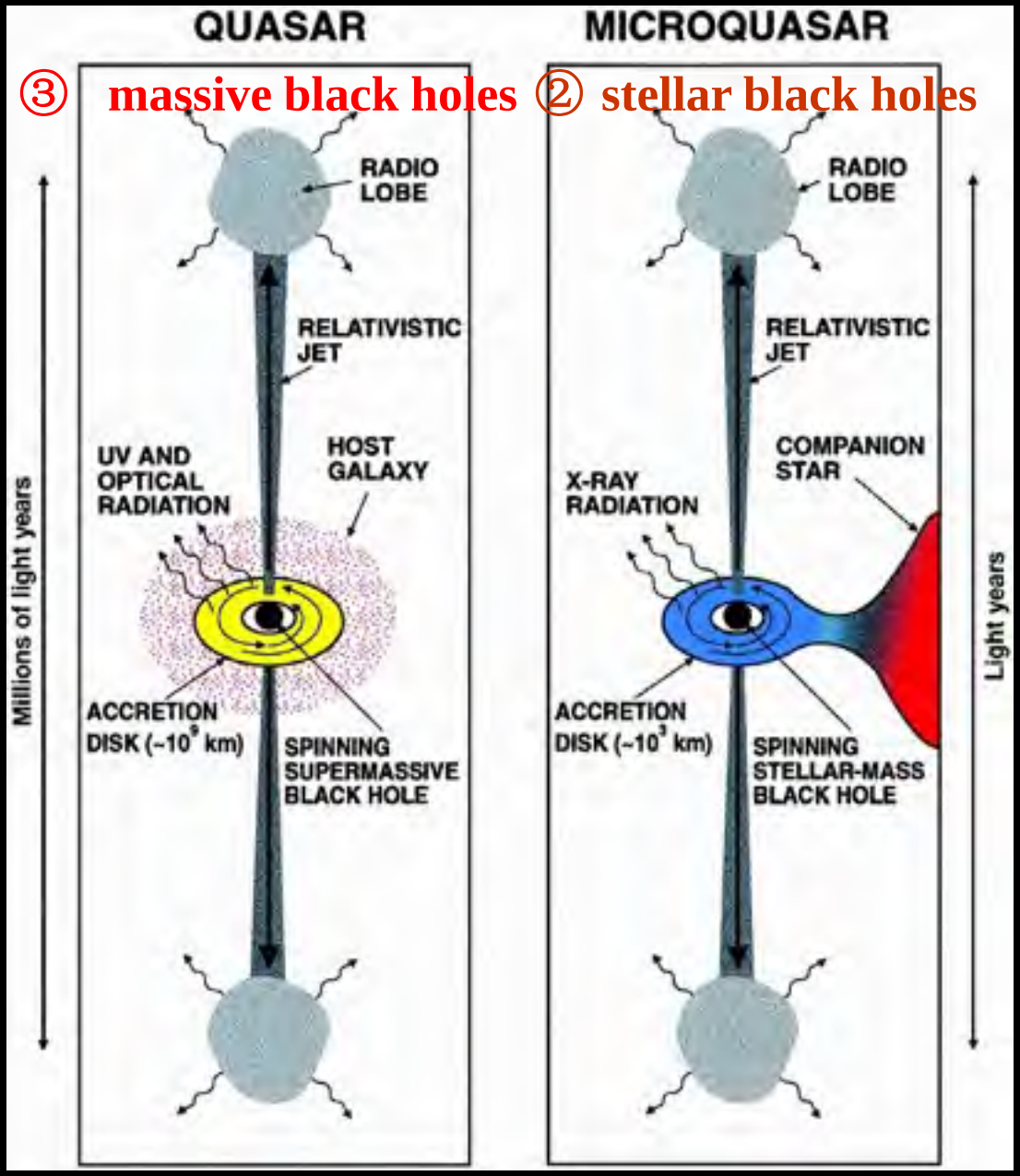

1. What are black holes?

prehistoric astronomy: “天似穹庐，笼盖四野”

astronomical models of the “universe”

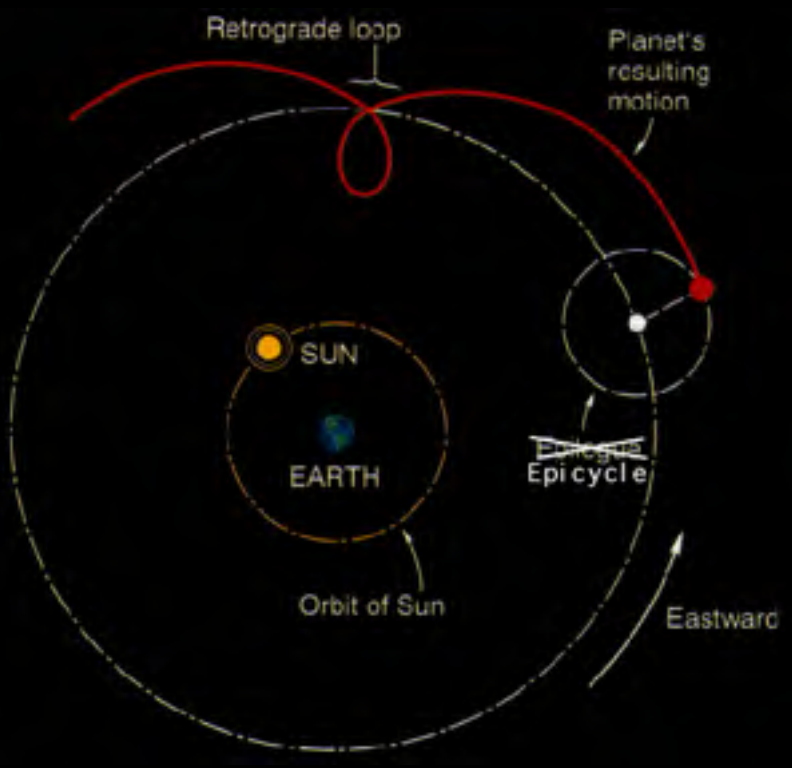

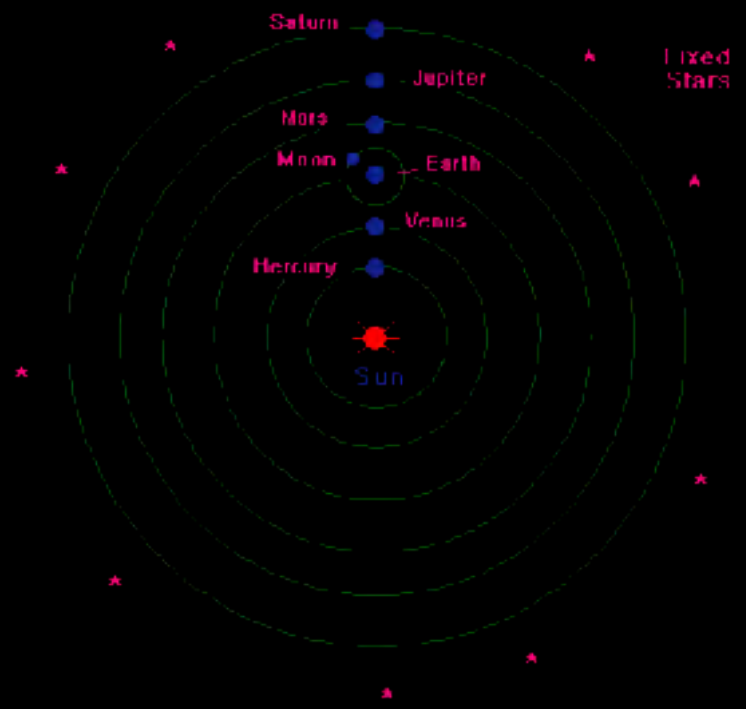

Pythagoras (582 - 500 BC)

Plato (428 - 347 BC)

Aristotle (384 - 322 BC):

“physics”

Hipparchus (190 - 120 BC); Copernicus (1473-1543)

Tycho (1546-1601), Kepler (1571-1630)

Newton (1642-1727):

“Philosophiae Naturalis Principia Mathematica”

Euclid (330 – 275 BC): “elements of geometry”: the 1st physics theory (R. Penrose)

cosmology today: "physics of astrophysics"

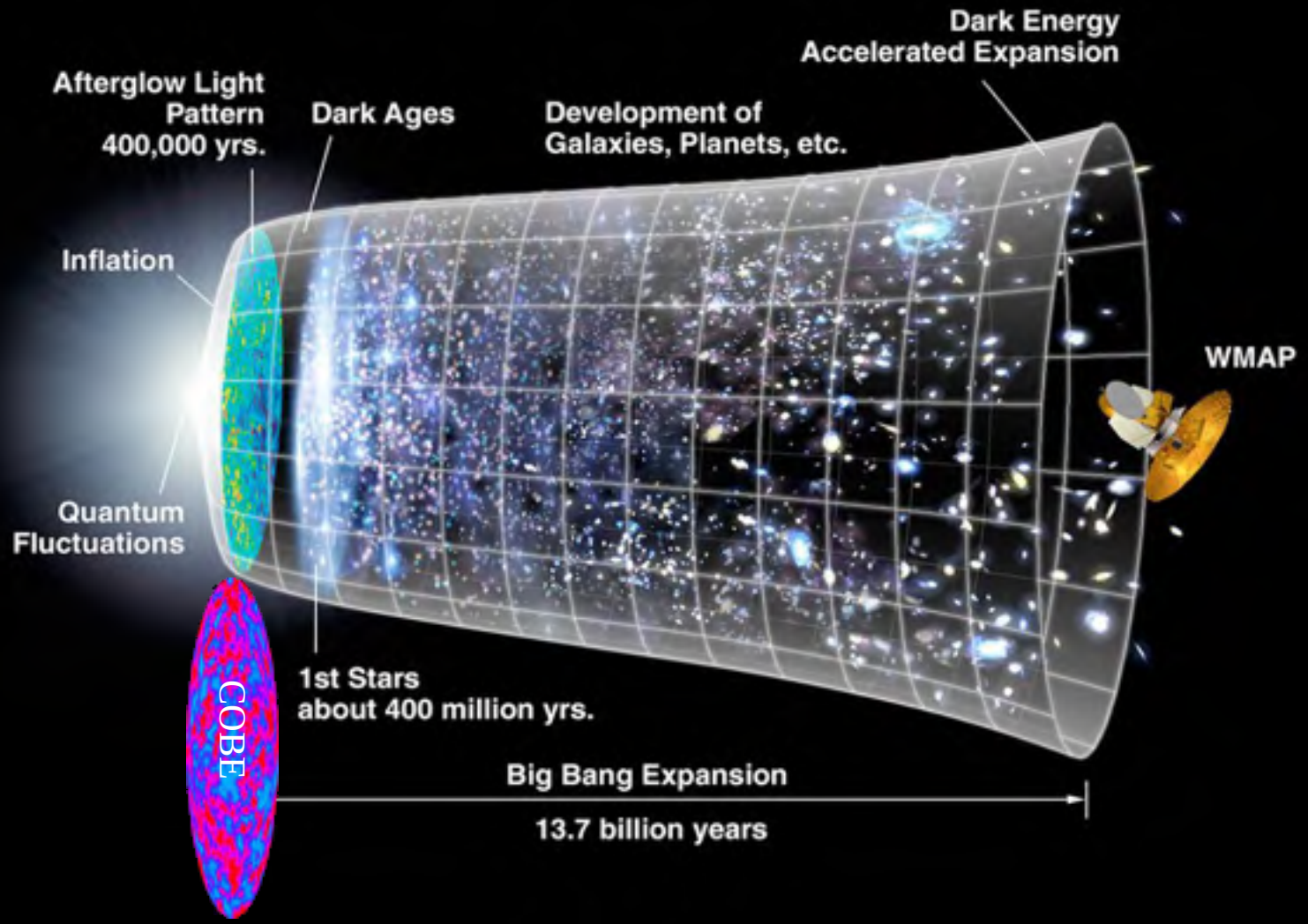

stars → galaxies ← universe; 2. Why BH inflows?

stellar structure: simple observational facts →
HR diagram → Vogt-Rusell conjecture

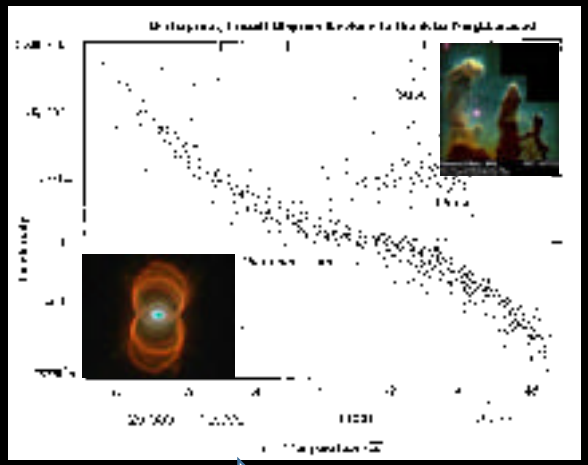

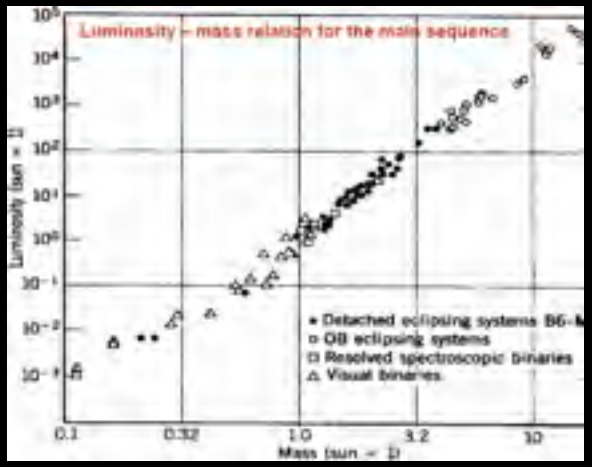

$$\begin{cases} p = p(\rho, T, Z), \\ \kappa = \kappa(\rho, T, Z), \\ \epsilon = \epsilon(\rho, T, Z); \end{cases}$$

$$\begin{cases} \dfrac{dp(r)}{dr} = -\dfrac{GM(r)\rho(r)}{r^2}, \\ \dfrac{dM(r)}{dr} = 4\pi r^2 \rho(r), \\ \dfrac{dT(r)}{dr} = -\dfrac{3L(r)\kappa(r)\rho(r)}{4\pi r^2 \cdot 4acT^3(r)}, \\ \dfrac{dL(r)}{dr} = 4\pi r^2 \rho(r)\epsilon(r). \end{cases}$$

galaxies ← **stellar evolution** ← cosmic **ecology**

nonlinear regime ← linear regime

big bang cosmology ← geometric cosmology

← Einstein: $R_{\mu\nu} - \frac{1}{2} R g_{\mu\nu} - \Lambda g_{\mu\nu} = \frac{8\pi G}{c^4} T_{\mu\nu}$

Almost all galaxies have experienced/ are going through AGN episodes !

1. **Anatomy of the AGN in NGC 5548.** I. A global model for the broadband spectral energy distribution (Mehdipour, M. et al. 2015)
2. **Anatomy of the AGN in NGC 5548. II**. The spatial, temporal, and physical nature of the outflow from HST/COS Observations (Arav, N. et al. 2015)
3. **Anatomy of the AGN in NGC 5548. III**. The high-energy view with NuSTAR and INTEGRAL (Ursini, F. et al. 2015)
4. **Anatomy of the AGN in NGC 5548.** IV. The short-term variability of the outflows (Di Gesu, L. et al. 2015)
5. **Anatomy of the AGN in NGC 5548.** V. A clear view of the X-ray narrow emission lines (Whewell, M. et al. 2015)
6. **Anatomy of the AGN in NGC 5548.** VI. Long-term variability of the warm absorber (Ebrero, J. et al. 2016)
7. **Anatomy of the AGN in NGC 5548.** VII. Swift study of obscuration and broadband continuum variability (Mehdipour, M. et al. 2016)
8. **Anatomy of the AGN in NGC 5548.** VIII. XMM-Newton's EPIC detailed view of an unexpected variable multilayer absorber (Cappi, M. et al. 2015)
9. **Anatomy of the AGN in NGC 5548.** IX. Photoionized emission features in the soft X-ray spectra (Mao, Junjie et al. 2018)

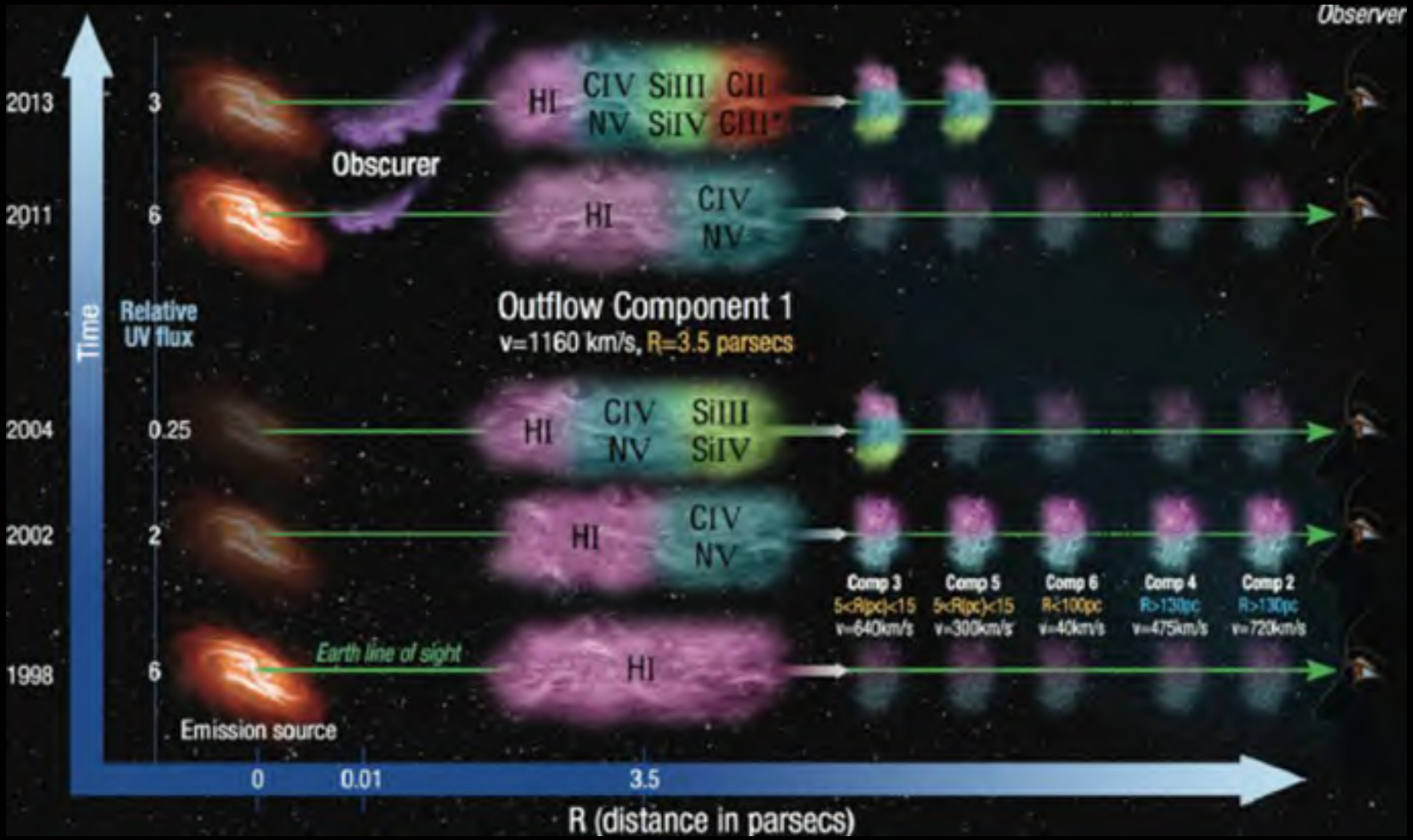

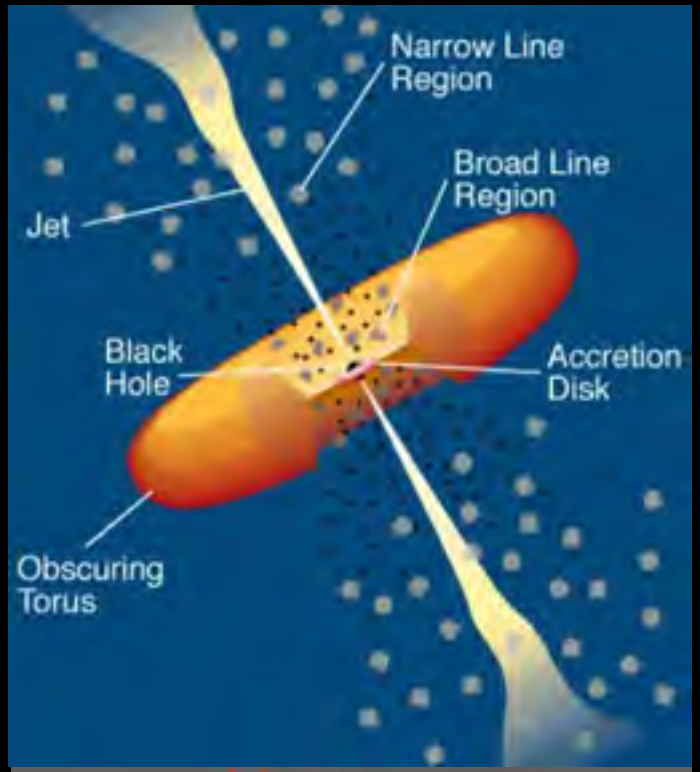

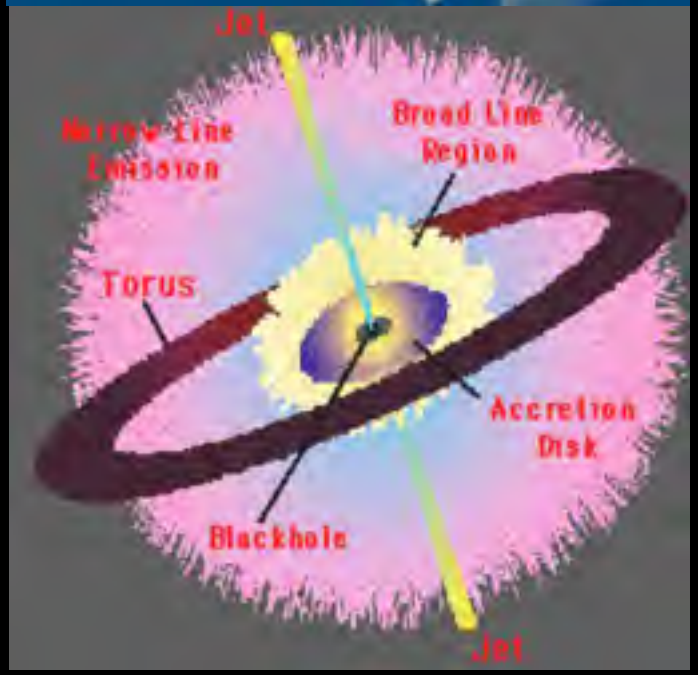

main analysis tools:

- ionic column-density extraction techniques;
- photoionization models;
- collisional excitation simulations.

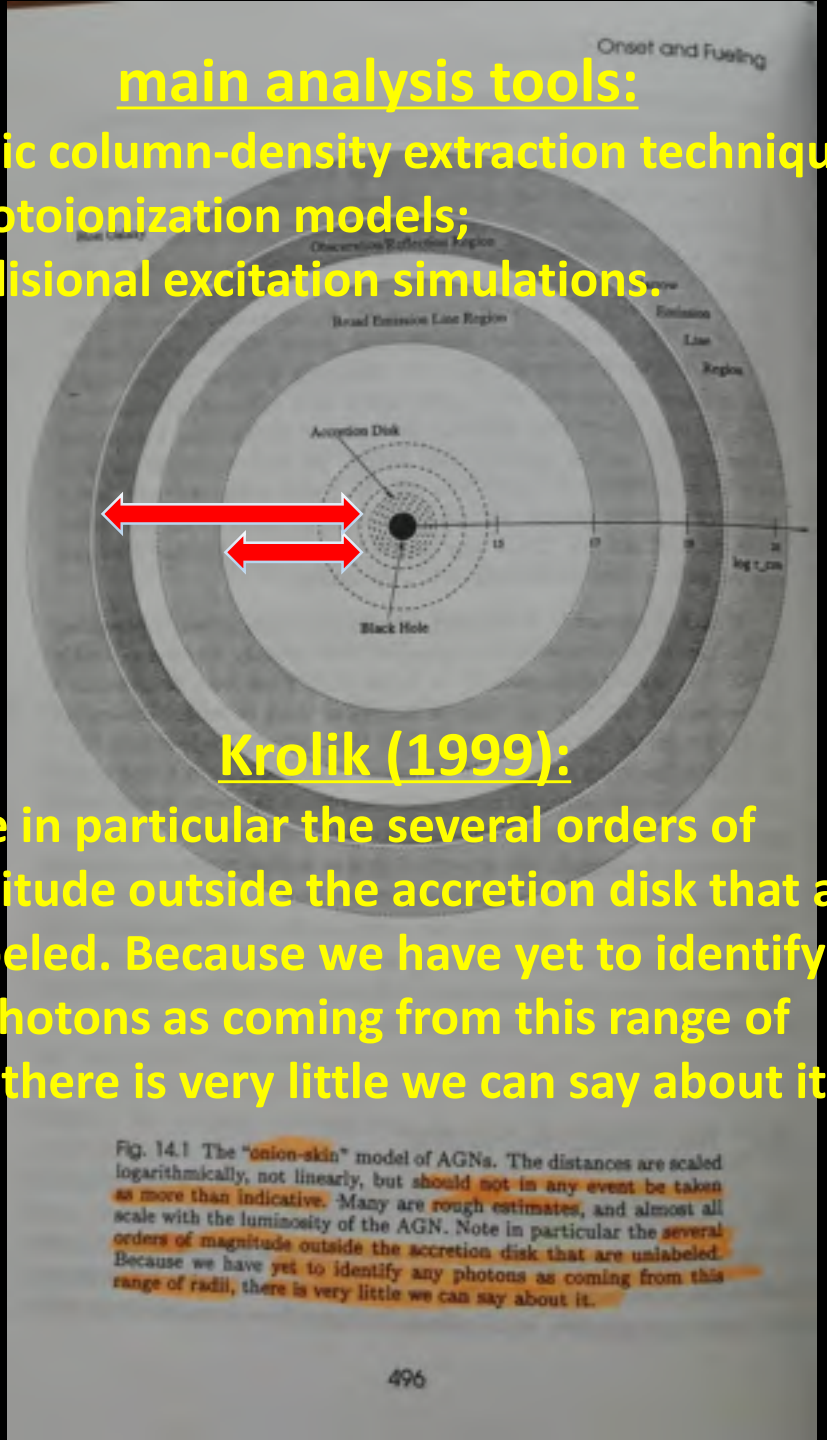

Krolik (1999):

"Note in particular the several orders of magnitude outside the accretion disk that are unlabeled. Because we have yet to identify any photons as coming from this range of radii, there is very little we can say about it."

Fig. 14.1 The "onion-skin" model of AGNs. The distances are scaled logarithmically, not linearly, but should not in any event be taken as more than indicative. Many are rough estimates, and almost all scale with the luminosity of the AGN. Note in particular the several orders of magnitude outside the accretion disk that are unlabeled. Because we have yet to identify any photons as coming from this range of radii, there is very little we can say about it.

496

accretion flows in quasars

- ISM inflows → galactic nuclear region（headstream✔）
- disk feeding inflows（**DFI?**）
- disk inflows（end✔）

3. how to track black hole accretion flows?

Bulian donkey effect ?

(1). EM or other(s)?

(2). lines or continuum?

(3). absorption or emission lines?

(3). absorption or emission lines?

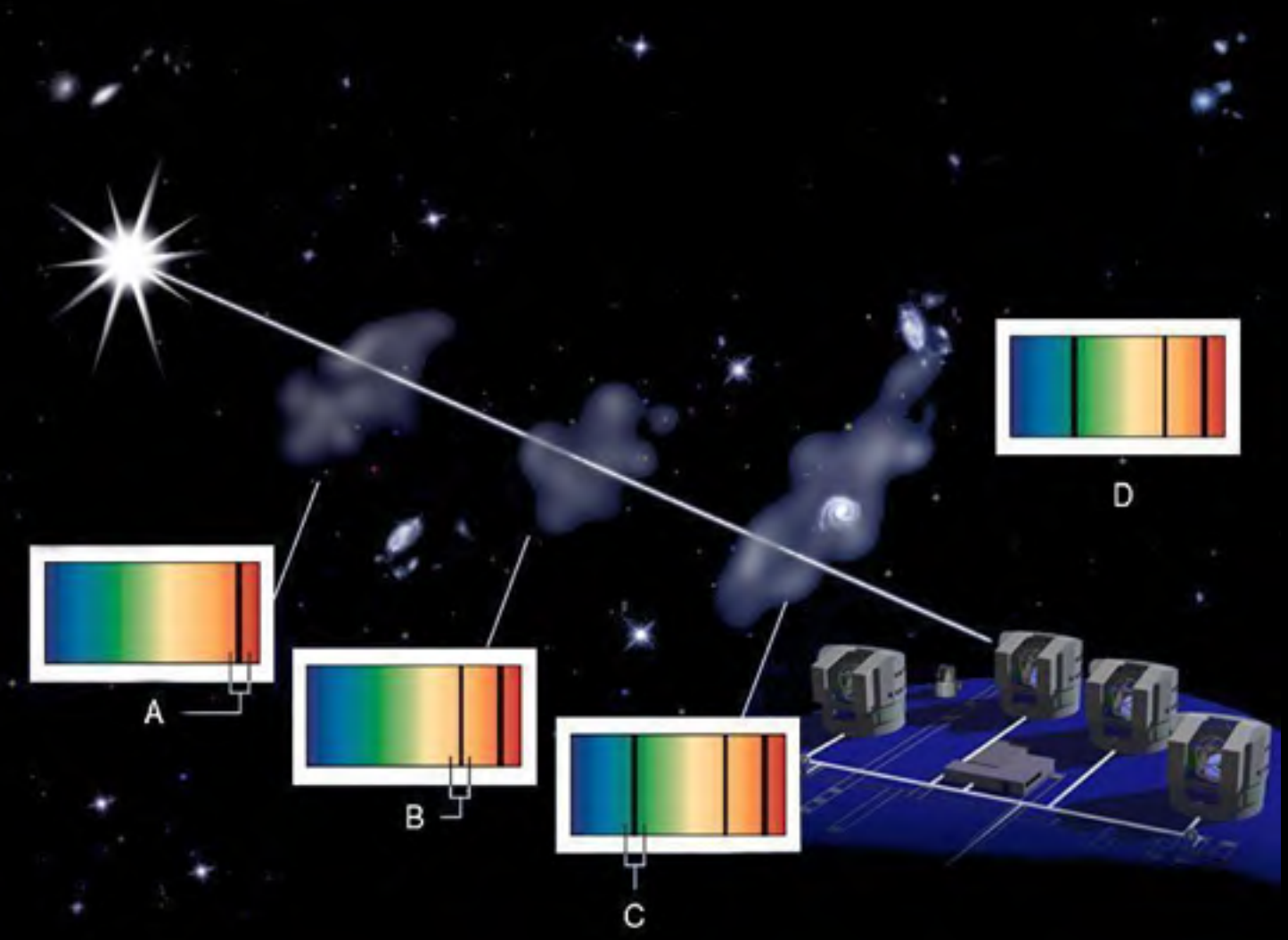

Radiative Transfer and Absorption Lines

Consider an incoming signal of a specific intensity, $I(v)$, passing through a gaseous slab, the intensity equals to photons gained and photons removed:

$dI = dI_{loss} + dI_{gain} \equiv -\alpha I dl + j dl.$

Define the absorption coefficient $\alpha \equiv \frac{d\tau}{dl}$, and consider only absorption, we have $dI = -I d\tau$.

Here τ is **optical depth**, which means the fraction of photons lost when the light passes a distance l. Solving the radiative transfer equation, $dI = -I d\tau$, we obtain $\int_{I_0}^{I} \frac{dI}{I} = \int_0^{\tau} d\tau$, i.e., $I = I_0 e^{-\tau}$. For a homogeneous medium, $\tau \propto l \propto N_H$, where N_H is the slab "thickness" parameterized as the total hydrogen ($H \equiv HI + HII$) column density. $I \propto F$, for parallel light.

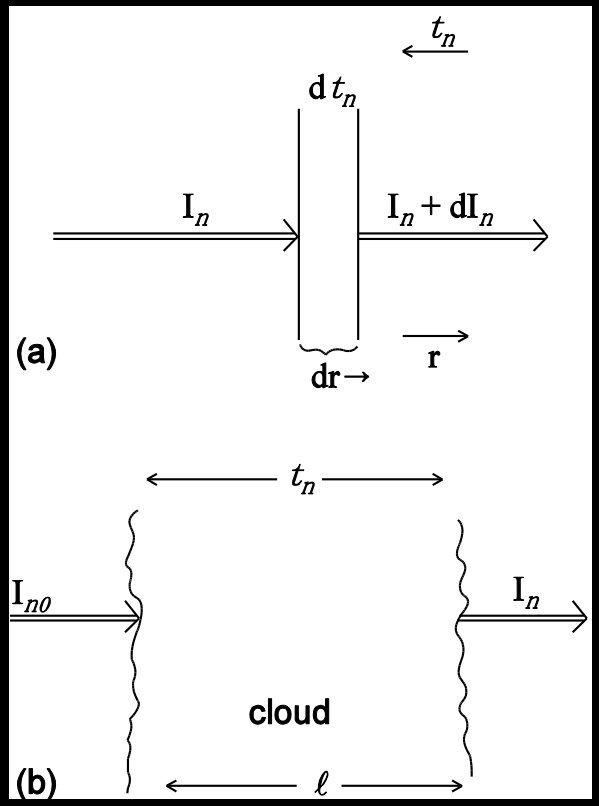

Assuming that the absorber is unsaturated and covers 100% of the emission region, we may calculate the column density of any ions by integration across the absorption-line profile (Savage & Sembach 1991):

$$N_X = \frac{m_e c}{\pi e^2 f_{ik} \lambda_0} \int \tau(v) dv = \frac{3.77 \times 10^{14}\ cm^{-2}}{\lambda_0 f_{ik}} \int \tau(v) dv.$$

(4). H/He or metal absorption lines?

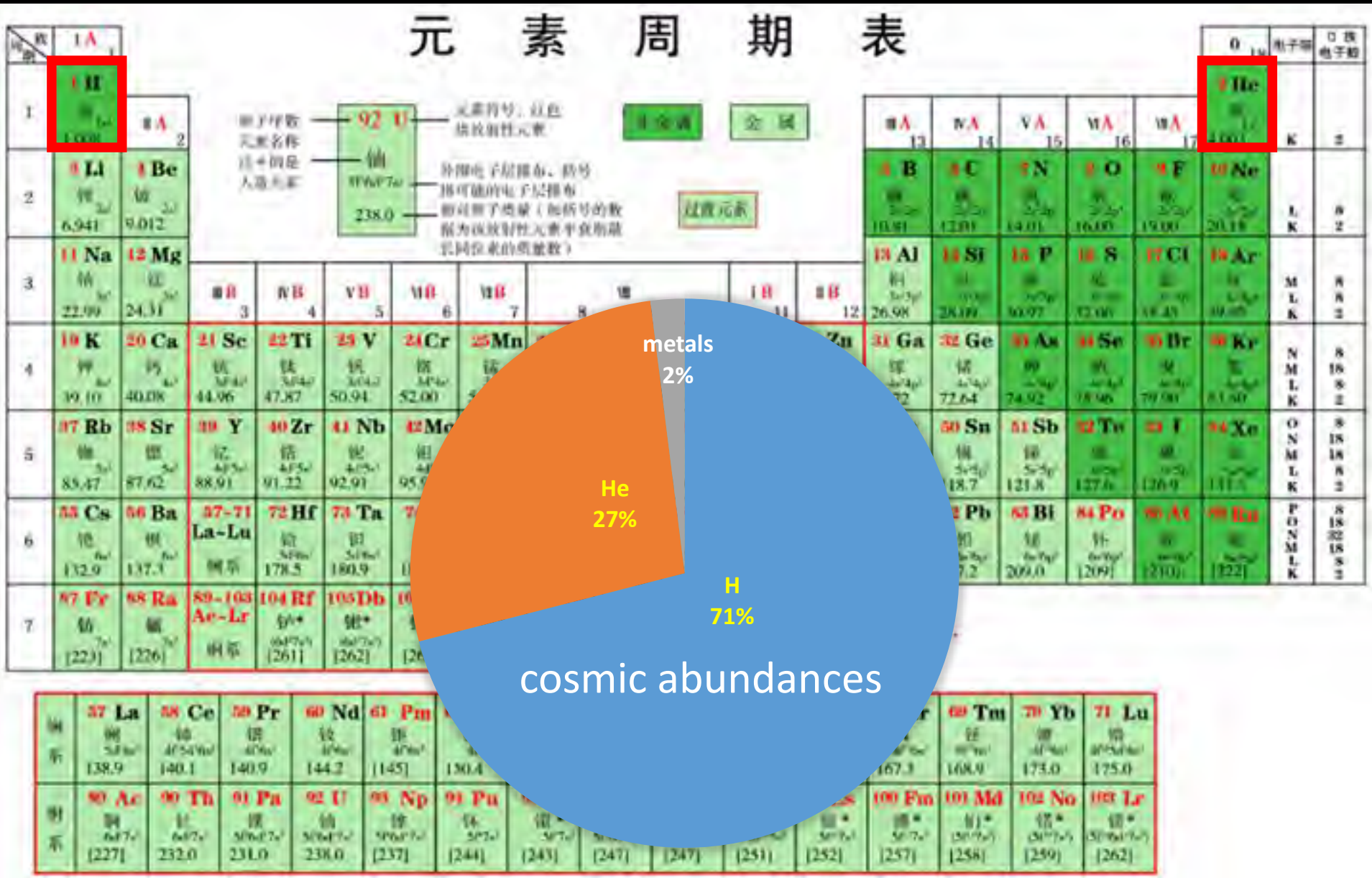

schematic energy levels of a hydrogen atom

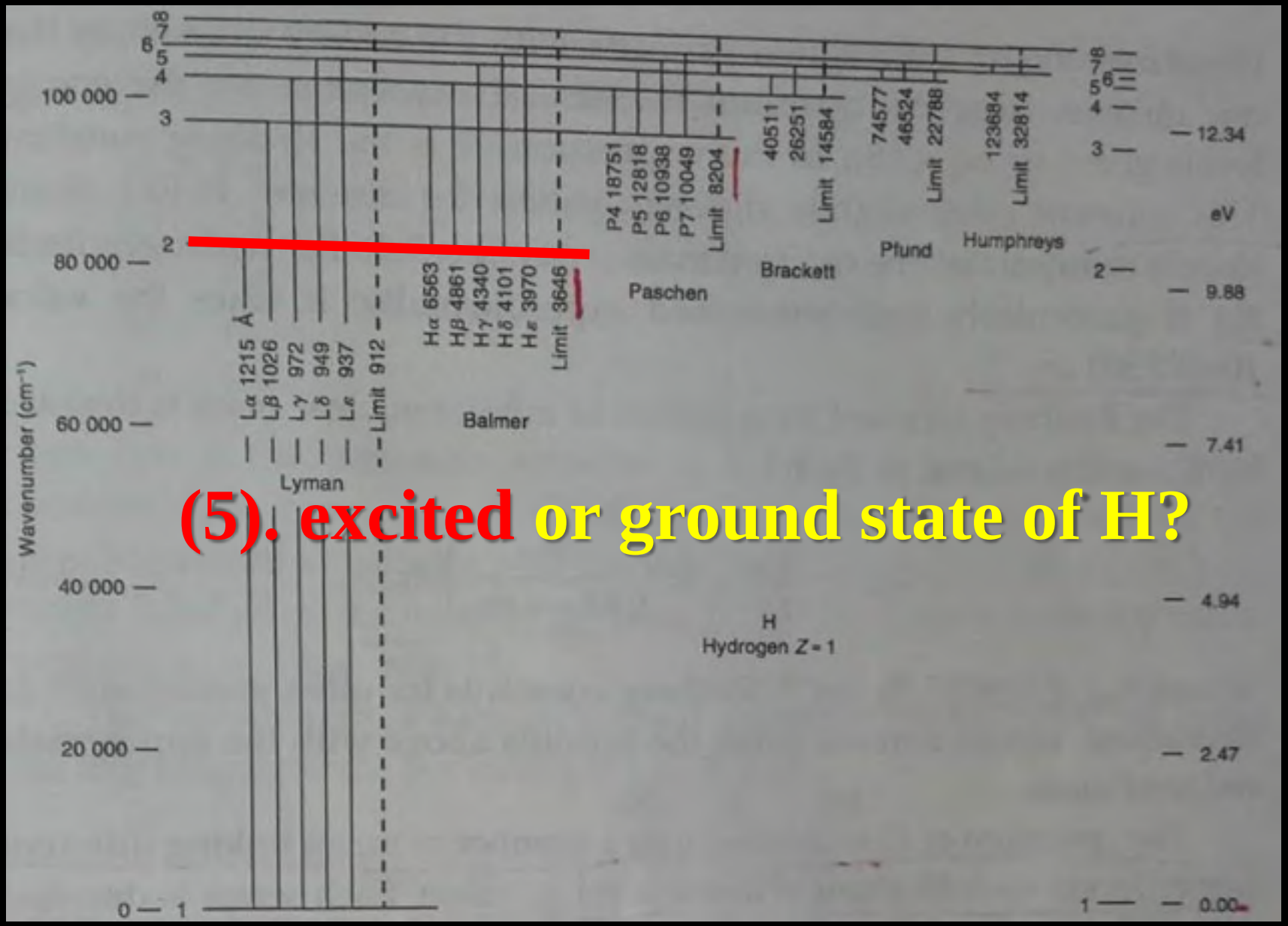

home works (introduction for astrophysics)

1. For a uniform cloud of pure hydrogen with temperature T and density n_H, determine the fraction of hydrogen atoms in the 1st excited state $\frac{n_{HI(n=2)}}{n_{HI}}$ as a function of temperature T and plot this function.
2. For the same cloud, determine the fraction of all hydrogen atoms that are ionized $\frac{n_{HII}}{n_{HI+HII}}$ as a function of T and $n_H \equiv n_{HI+HII}$, and plot this function for $n_H = 10^2 \; and \; 10^{10} cm^{-3}$.
3. For $n_H = 10^6 - 10^{12} cm^{-3}$, determine and plot $\frac{n_{HI(n=2)}}{n_H}$ as a function of T.

Solution:

1. The ratio is determined by the Boltzmann equation, if LTE holds, i.e.,

$$\frac{n_{HI(n=2)}}{n_{HI}} = \frac{g_2}{g_1}\exp\left[-\frac{\Delta E(n=1\leftrightarrow n=2)}{k_B T}\right] = \frac{2\cdot 2^2}{2\cdot 1^2}\exp\left[-\frac{(1-1/2^2)13.6eV}{8.62\times10^{-5}eVK^{-1}T}\right] = 4\exp\left[-\frac{11.83}{T/10^4K}\right]$$

2. According to the Sahar equation, $\frac{n_{HII}}{n_{HI+HII}} = \frac{2U_{1+1}}{n_e U_1}\left(\frac{2\pi m_e k_B T}{h^2}\right)^{3/2}\exp\left(-\frac{\Delta E_1}{k_B T}\right) = 2.41\times10^{11}\frac{(T/10^4K)^{3/2}}{(n_e/10^{10}cm^{-2})}\exp\left[-\frac{15.77}{T/10^4K}\right]$.

3. $\frac{n_{HI(n=2)}}{n_H} = \frac{n_{HI(n=2)}}{n_{HI}} \times \frac{n_{HII}}{n_{HI+HII}}$.

the 1st excited state of HI

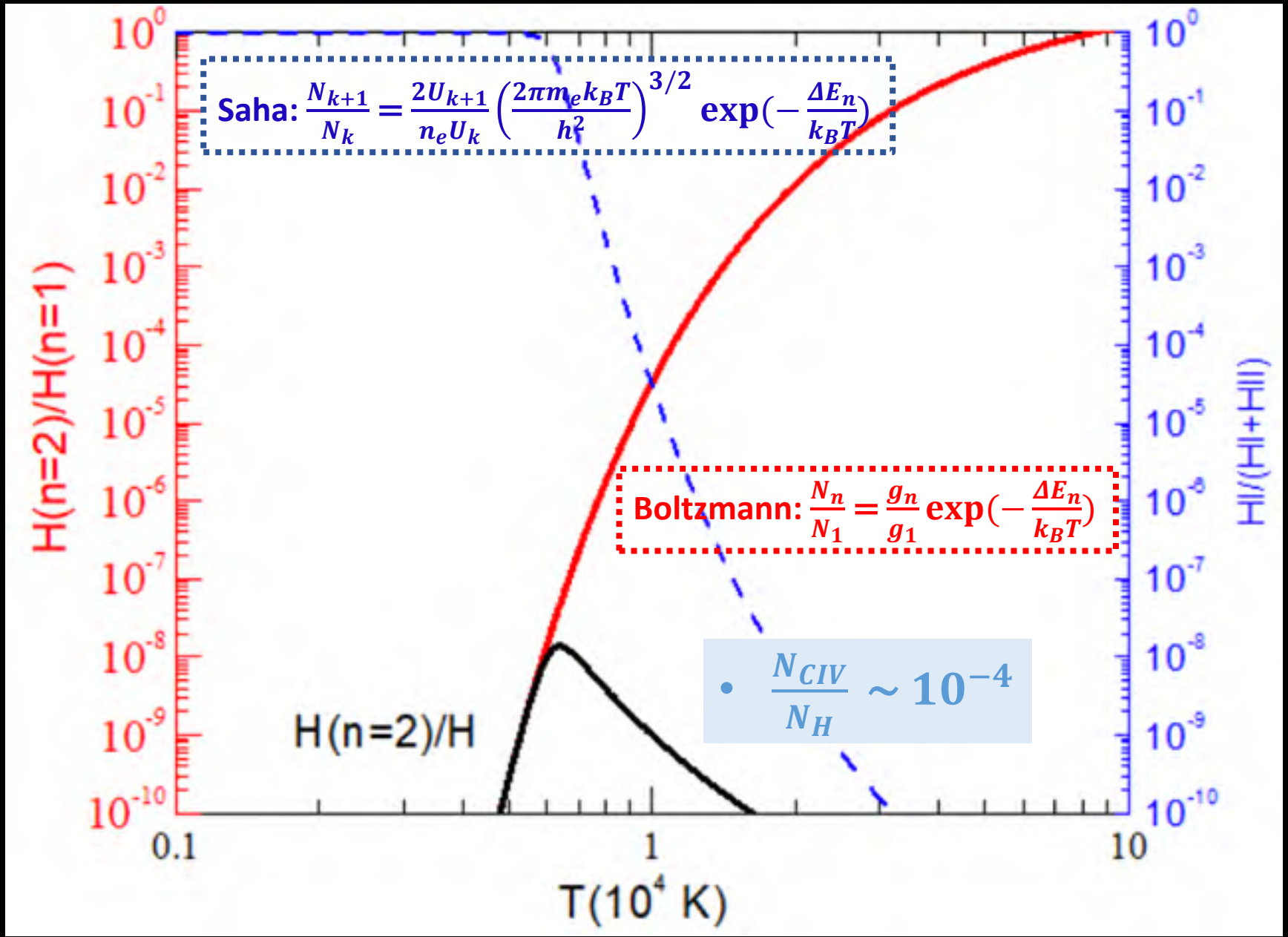

Grotrian diagram for a helium atom

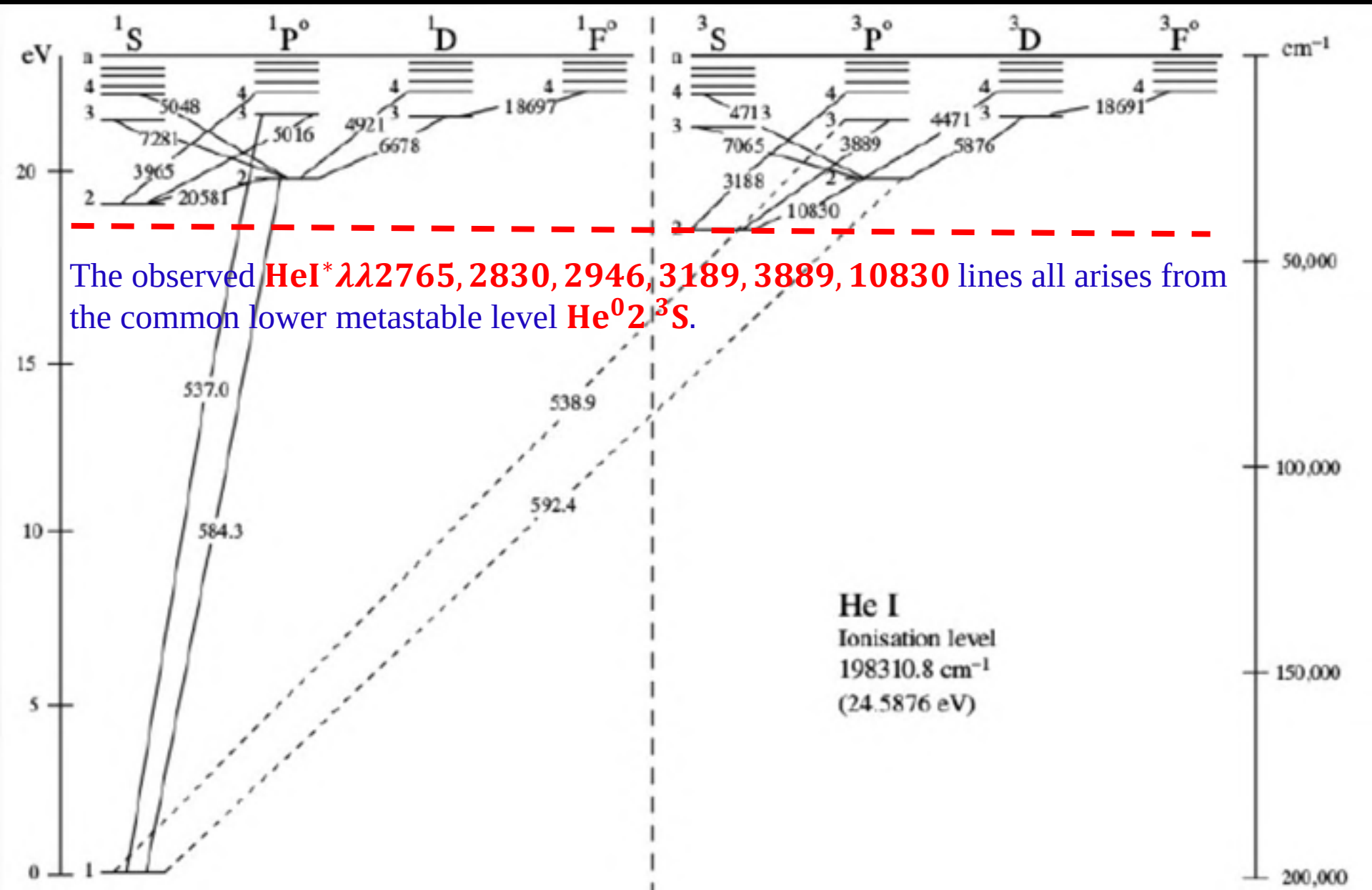

The observed $\mathbf{HeI^{*}\lambda\lambda 2765, 2830, 2946, 3189, 3889, 10830}$ lines all arises from the common lower metastable level $\mathbf{He^{0}2\,^{3}S}$.

Physics of HeI* absorption line multiplets

In equilibrium, the population of the $2\ ^3S$ is determined by the balance of arrivals from recombination to all triplet levels versus departures mainly due to collisional transition to other levels. Under most conditions all recombinations to the triplet levels end up in the $2\ ^3S$ level, the total recombination coefficient is $\alpha_T \approx \alpha\ (He^0\ 2\ ^3S) + \alpha\ (He^0\ 2\ ^3P^o)$; and

$$n_{He^+} \cdot n_e \cdot \alpha_T = n_{2\ ^3S}\left[A_{21} + n_e(q_{ct} + q_{ci}) + \int_{\nu_0}^{\infty} \frac{\alpha_\nu L_\nu}{4\pi r^2 h\nu}\, d\nu\right],$$

where n_{He^+} is the number density of He^+ions, n_e is the electron number density, α_T is the total recombination coefficient to all triplet levels, $n_{2\ ^3S}$ is the number density of neutral helium in the $2\ ^3S$ level, A_{21} is the Einstein A-coefficient for the forbidden transition (625 Å) from the $2\ ^3S$ level to the ground level ($1\ ^1S$), q_{ct} is the rate of collisional transfer to all singlet level (which is dominated by collisions to the $2\ ^1S$ and $2\ ^1P$ levels), q_{ci} is the collisional ionization rate which becomes important above 20,000 K (Clegg 1987), α_ν is the photoionization cross section for $2\ ^3S$, L_ν is the spectral luminosity and r is the distance to the emitting source, h is Planck's constant, and ν_0 is the threshold frequency for ionizing the $2\ ^3S$ level (4.77 eV or 2600 Å).

Including radiative transition to the ground level but neglecting photoionization, we may have a good approximation of (for $8 \times 10^3 < T < 2 \times 10^4$; Clegg 1987):

$\frac{n_{2\ ^3S}}{n_{He^+}} = \frac{5.8\times10^{-6} T_4^{-1.19}}{1+3.11\times10^3 T_4^{-0.51} n_e^{-1}}$, where T_4 is the temperature in units of 10^4 K.

Physics of HeI* absorption line multiplets

If $n_e > 3 \times 10^3 cm^{-3}$(the critical density), the effects of photoionization, collisional ionization and radiative transition to the ground level, can be neglected, we only need to consider *recombination* and the *collisional transfer to the singlet level*, and thus can further simplify the ratio as

$$\frac{n_{2\,^3S}}{n_{He+}} = \frac{q_{ct}}{\alpha_T} = 6 \times 10^{-6}.$$

Typically, $N_{He^0\,2\,^3S} = \frac{3.77\times10^{14}\ cm^{-2}}{\lambda_0 f_{ik}} \int \tau(v)dv \sim \frac{3.77\times10^{14}\ cm^{-2}}{3889.74\cdot0.064} \cdot 10^{3-4} \sim 10^{15-16} cm^{-2}$, $N_{He^+} \sim 2 \times 10^{20-21}\ cm^{-2}$. Assuming solar abundances this estimate yields a minimal H II column density of $N_{H^+} > 2 \times 10^{21-22}\ cm^{-2}$. Higher order **HeI*** absorption lines can probe $\sim 2-3$ orders of magnitude higher column densities (up to **Compton thick**).

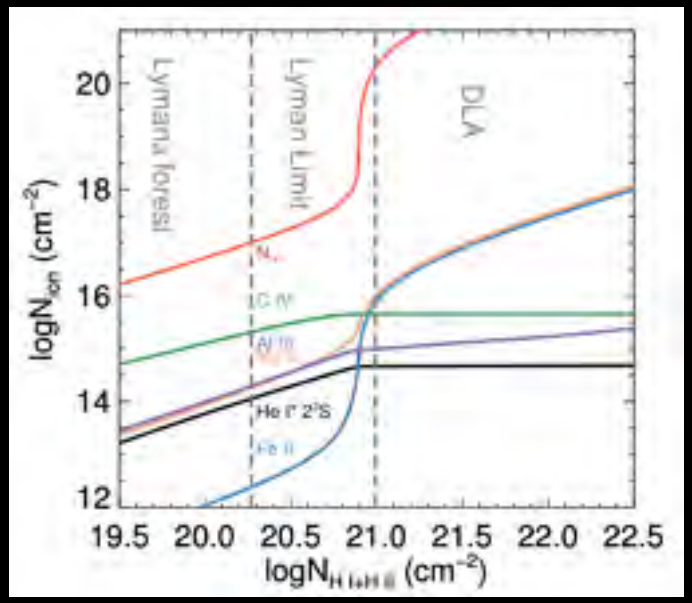

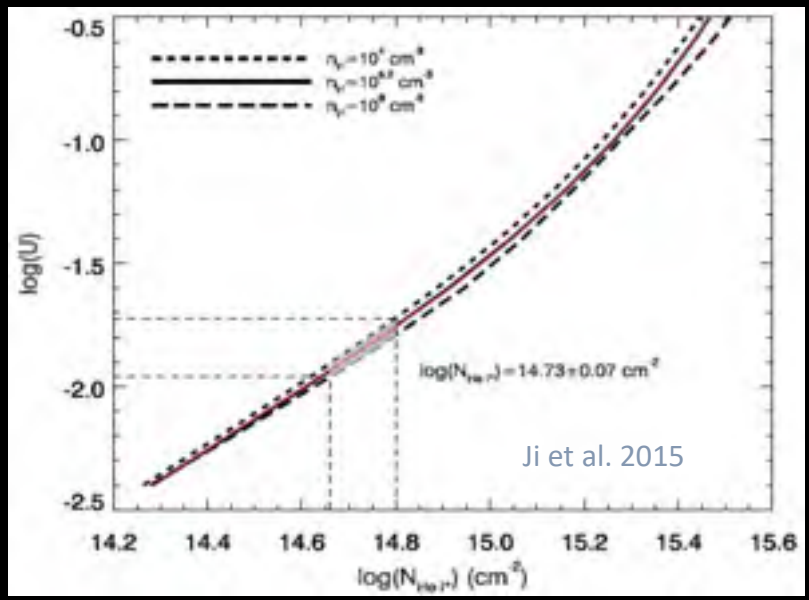

ionization structure of quasar intrinsic absorbers

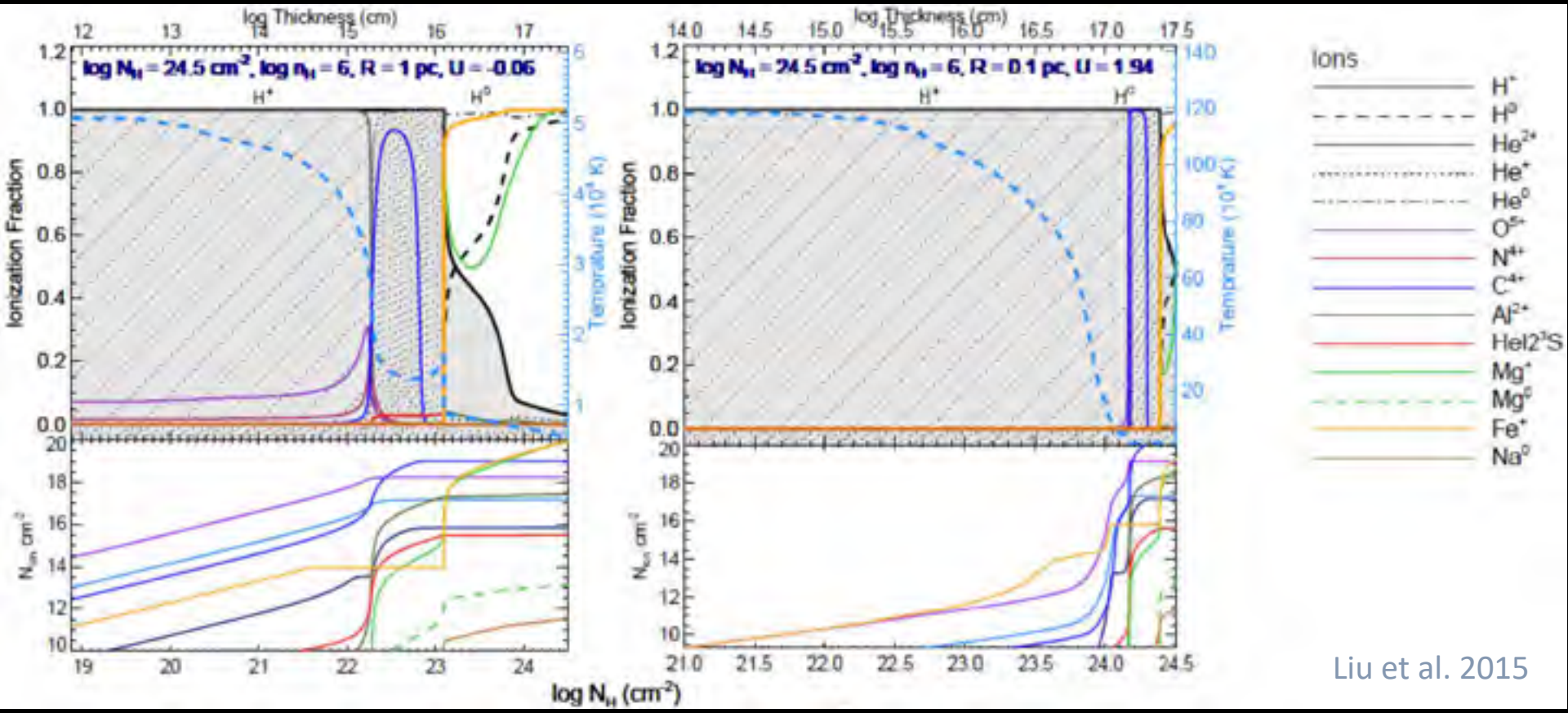

Liu et al. 2015

- $\frac{N_{HeI*}}{N_H} \sim 6 \times 10^{-7}$
- $\frac{N_{HI*(n=2)}}{N_H} \sim 10^{-7}$

- $\frac{N_{CIV}}{N_H} \sim 10^{-4}$
- $\frac{N_{MgII}}{N_H} \sim 10^{-5}$

diagnosability of H Balmer and HeI* absorption lines

$1-10\ M_{\odot} yr^{-1} \sim \dot{M} = 4\pi r \cdot \Omega \cdot \mu \cdot m_p \cdot N_H \cdot v \rightarrow \boldsymbol{N_H \sim 10^{23-25} cm^{-1}}$

(for **in/outflows** with $\Omega \sim 10\%$, v~3,000 km s^{-1}; r ~0.1-1pc)

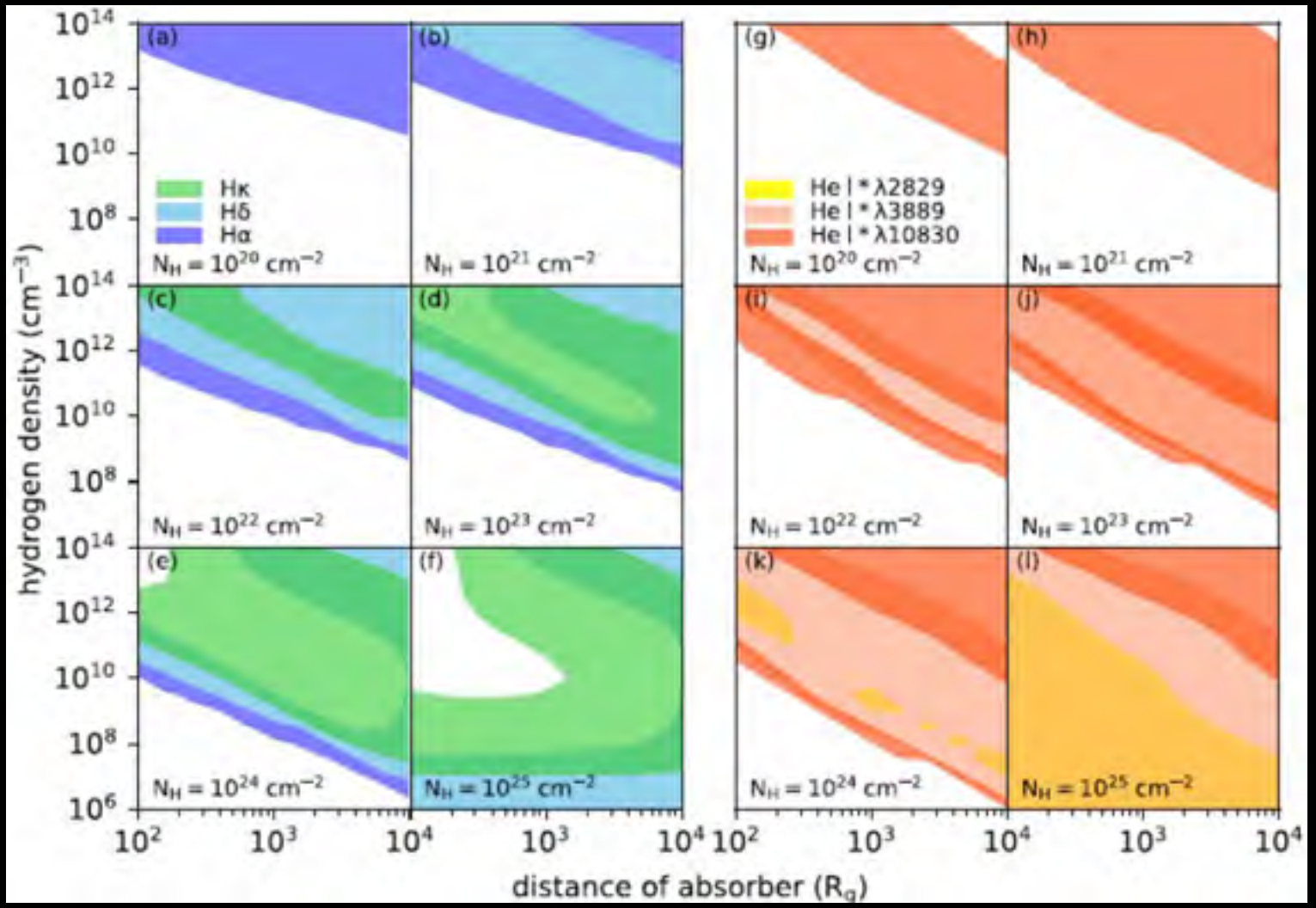

prep. works

1. Zhang et al. 2010, Low-z **Mg II** Broad Absorption-line Quasars from SDSS
2. Ji et al. 2012, Discovery of **Balme**r broad absorption lines in the quasar LBQS 1206+1052
3. Ji et al. 2013, **Balmer** Absorption Line Spectrum of Quasar SDSS J2220+0109
4. Liu et al. 2015, Prevalence of **HeI*** Absorption Line Multiplets in **Mg II** Low-ionization Objects
5. Zhang et al. 2015, Discovery of Extremely Broad **Balmer** Absorption Lines in SDSS J1523+3914
6. Shi et al. 2016, Broad **Balmer** Absorption Line Variability
7. Jiang et al. 2016, Strong **Lyα Emission** in the **Proximate Damped Lyα Absorption** Trough
8. **Shi et al. 2016, Redshifted Hydrogen Balmer and Metastable HeI* Absorption Line System**
9. Pan et al. 2017, Intrinsic Dusty Absorber with a Metal-rich **Damped Lyα** Absorption Line System
10. Sun et al. 2017, Variability in **Balmer Absorption Line** Quasar
11. Shi et al. 2017, Variable **Hydrogen Balmer Absorption Lines with Inverse Decrement**
12. Zhang et al. 2018, Ultra-dense Broad-line Region Scale Outflow
13. Pan et al. 2018, Scattered Continuum in the Lyman Limit Absorption Edge

…

- Tian et al. 2019, Galactic-scale Broad Absorption Line Outflow
- Pan et al. 2019, Metastable **He I* λ10830** Absorption and Very Narrow **Paschen α** Emission Lines
- Li et al. 2020, **Ultradense Gas at the Dusty Torus Scale** in a Partially Obscured Quasar

…

France Bacon: "the cripple but not lost can surpass the people who walk fast but in a wrong road."

4. a case study of J1035+1422

刘万东：“氢氦红移流速定”

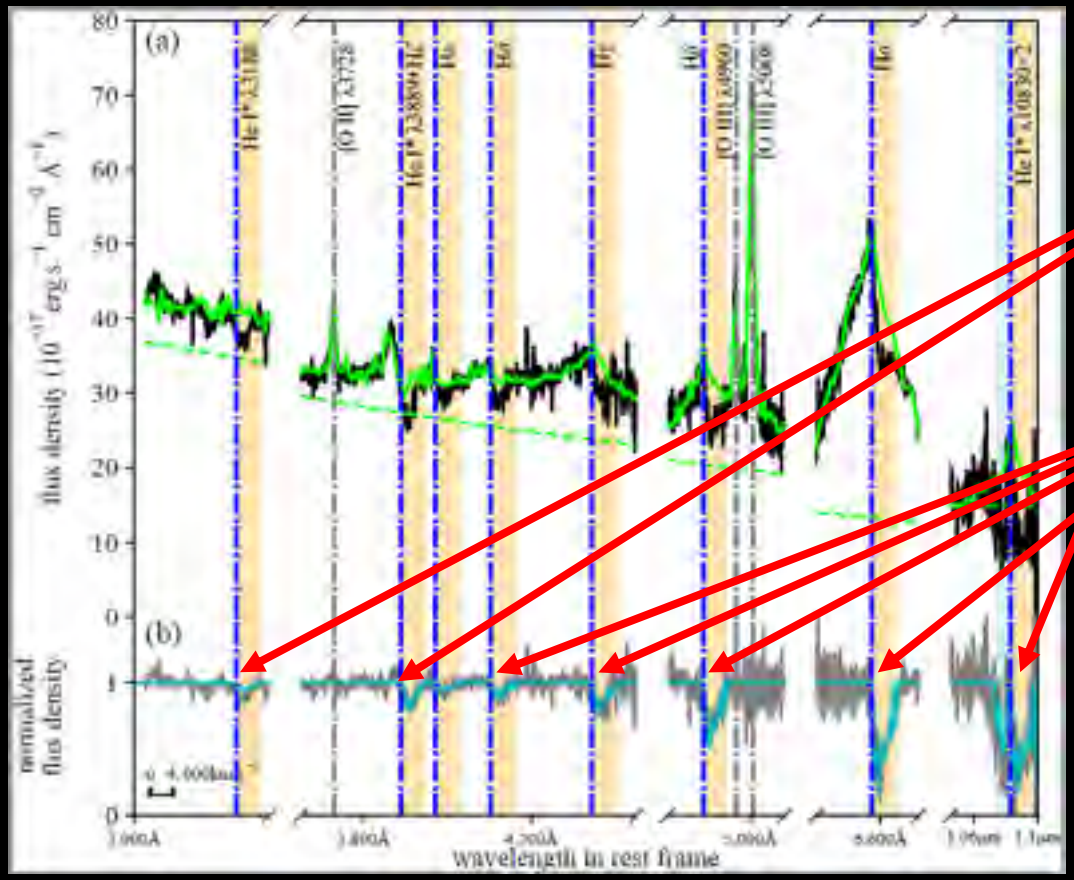

meta-stable HeI*

HI* Balmer

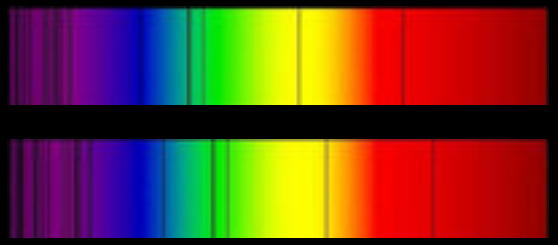

多普勒红移

Doppler redshift up to 5,000 km/s → $r < 7{,}200\ r_g$

inflow distance constrained by the simple physics of gravity

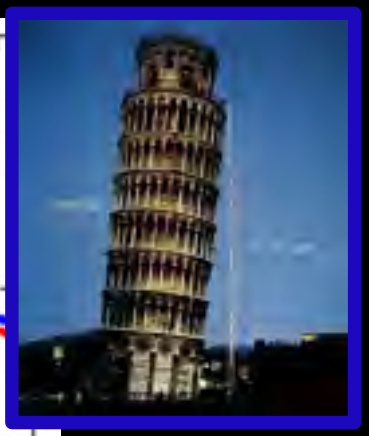

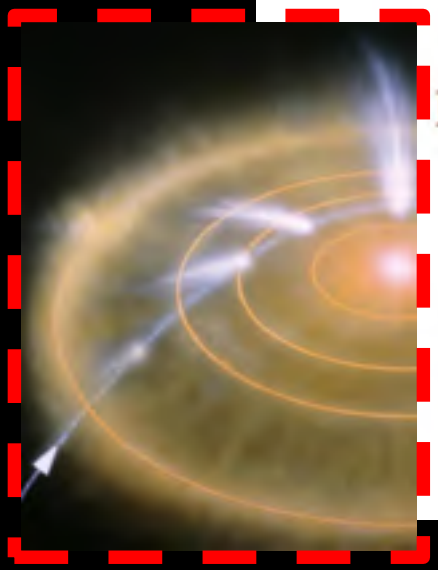

$$\begin{cases} \textit{conservation of angular momentum,} \\ \textit{conservation of mechanical energy.} \end{cases}$$

5,000 km/s → $r < 7,200\ r_g$,
very possibly $r < 3,600\ r_g$;
finally → $r < 1,000\ r_g$

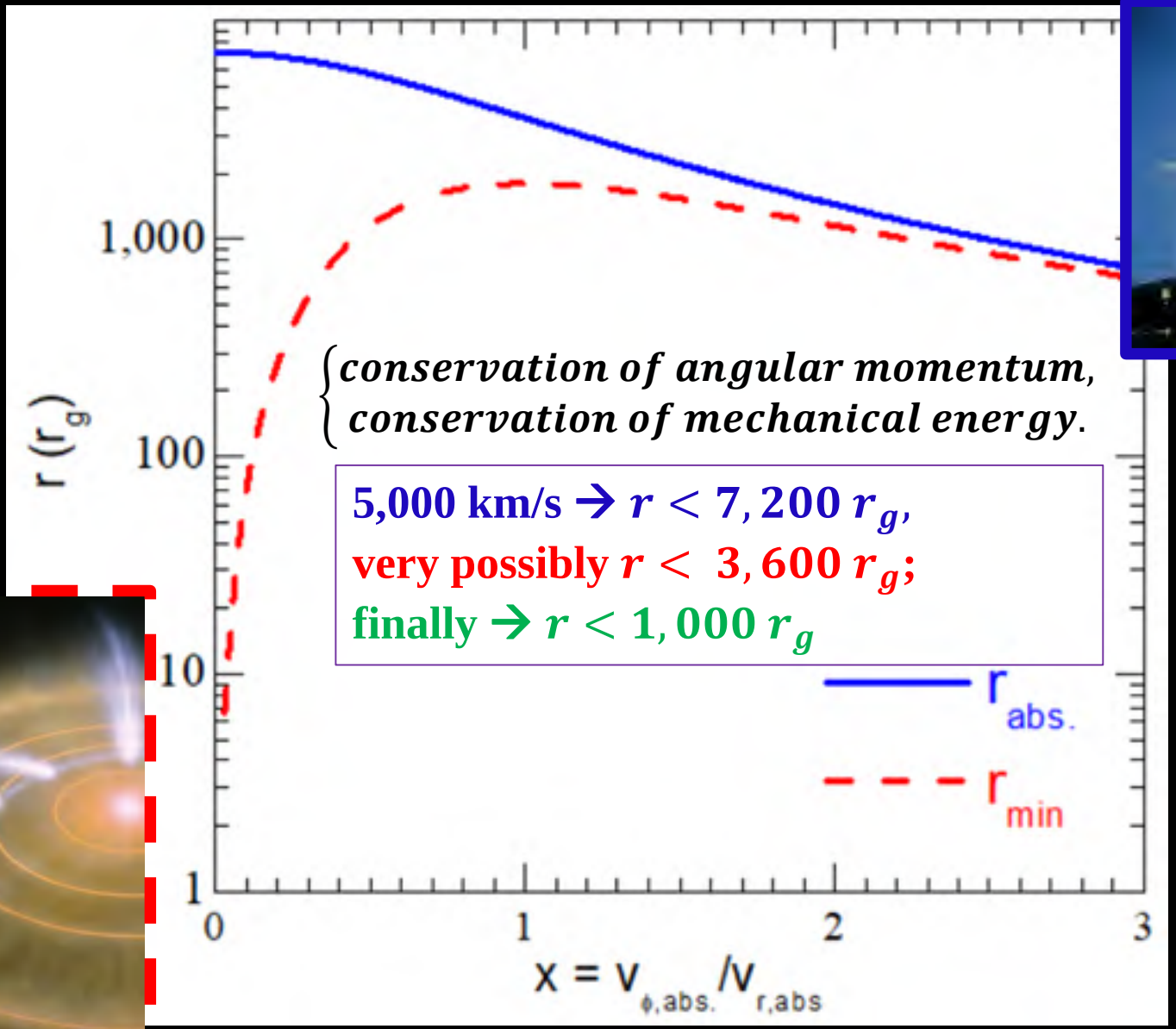

J1035+1422: isolated BALs in velocity space

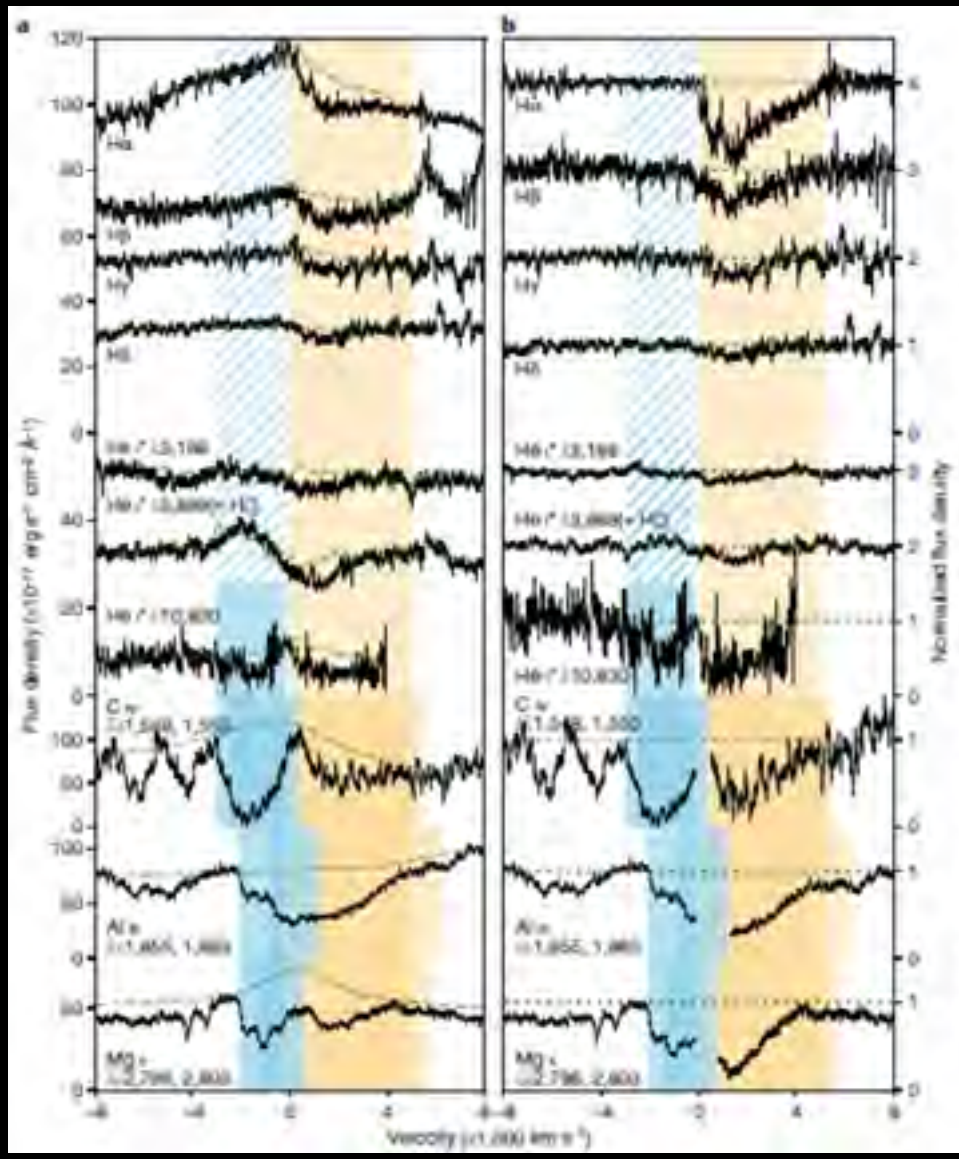

Fig. 2 | Close-up of the absorption spectrum of J1035 + 1422 in selective hydrogen, helium and metal lines. **a**, Observed flux density. **b**, Normalized flux density. The velocity ranges for the redshifted and blueshifted broad-absorption-line systems (regions coloured in orange and blue, respectively) are determined according to the normalized Hα and He I* λ10,830 broad absorption-line spectra. The seeming velocity differences between the H I*, He I* and metal lines are mostly due to the fact that all of the metal lines are actually doublets, with velocity offsets of 500 km s^{-1}, 1,300 km s^{-1} and 770 km s^{-1} between the two member lines of C IV, Al III and Mg II, respectively. The best-fit quasar composite spectrum is shown by the green dashed lines. It is obvious that the redshifted C IV trough is shallower than the blueshifted C IV trough and than the redshifted Mg II and Hα troughs. The He I* λ3,889 line is severely blended with H I λ3,890, with a measured optical depth ratio of 0.7/0.3. Note that all of the H I* and He I* lines show solely redshifted absorption troughs except for He I* λ10,830, which is the strongest of the multiplets[10]. This implies a drastically distinctive physical condition of the redshifted broad-absorption-line gas from that of the blueshifted one. Unlike emission lines, which may be complicated by various effects, such as obscuration and projection, redshifted absorption lines are clean in kinematics and are a robust indication of inward motion of the absorbing gas along the line of sight[9].

Hα optical depth and covering fraction

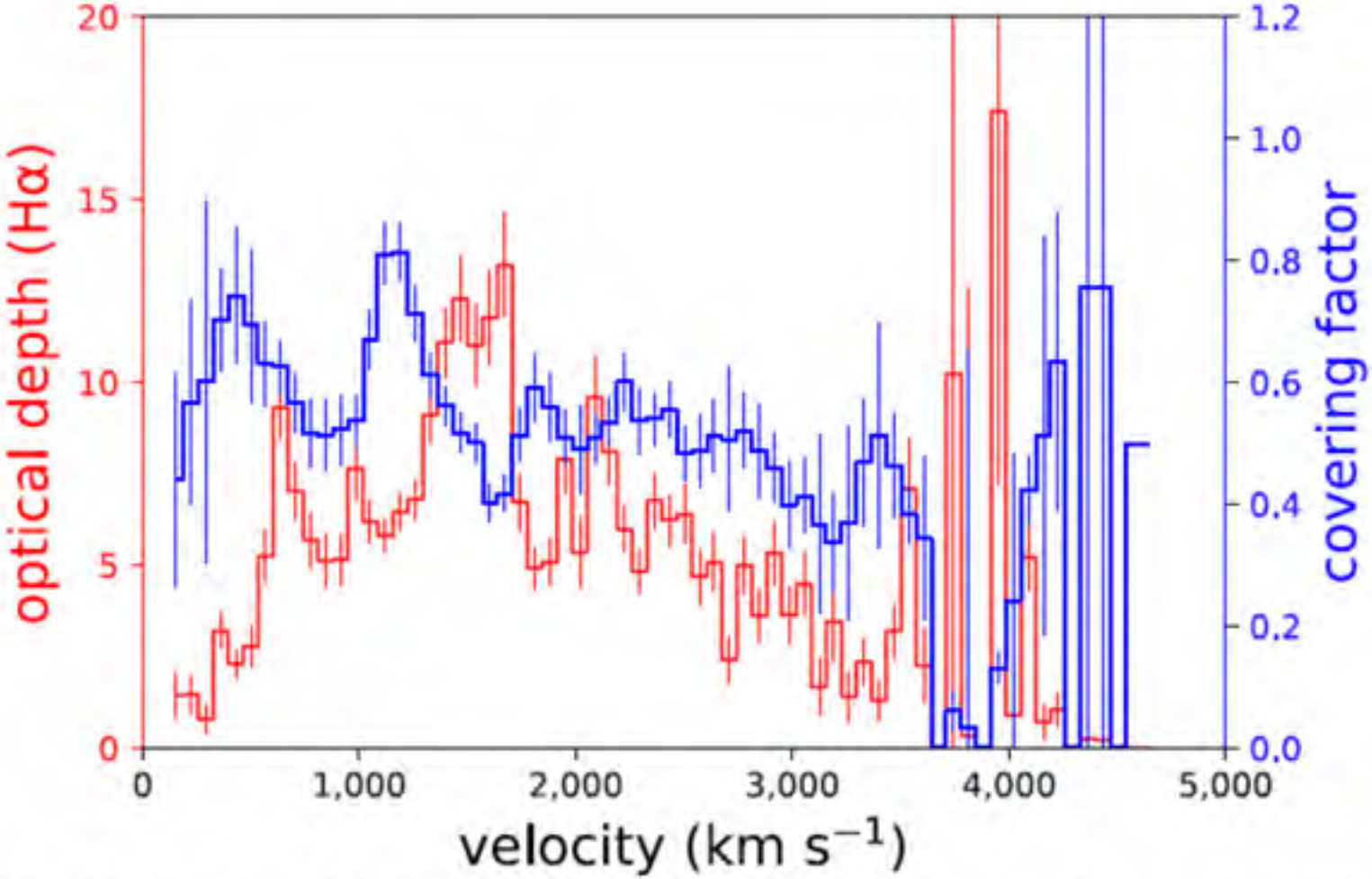

Extended Data Fig. 4 | Velocity structure of the redshifted Hα broad absorption line of J1035 + 1422. The optical depth (red) and local covering factor (blue) of the line, derived from the continuum-normalized spectrum, are shown as a function of velocity shift with respect to the quasar's rest frame. The error bars represent 1σ uncertainties.

anomalous metal absorption lines

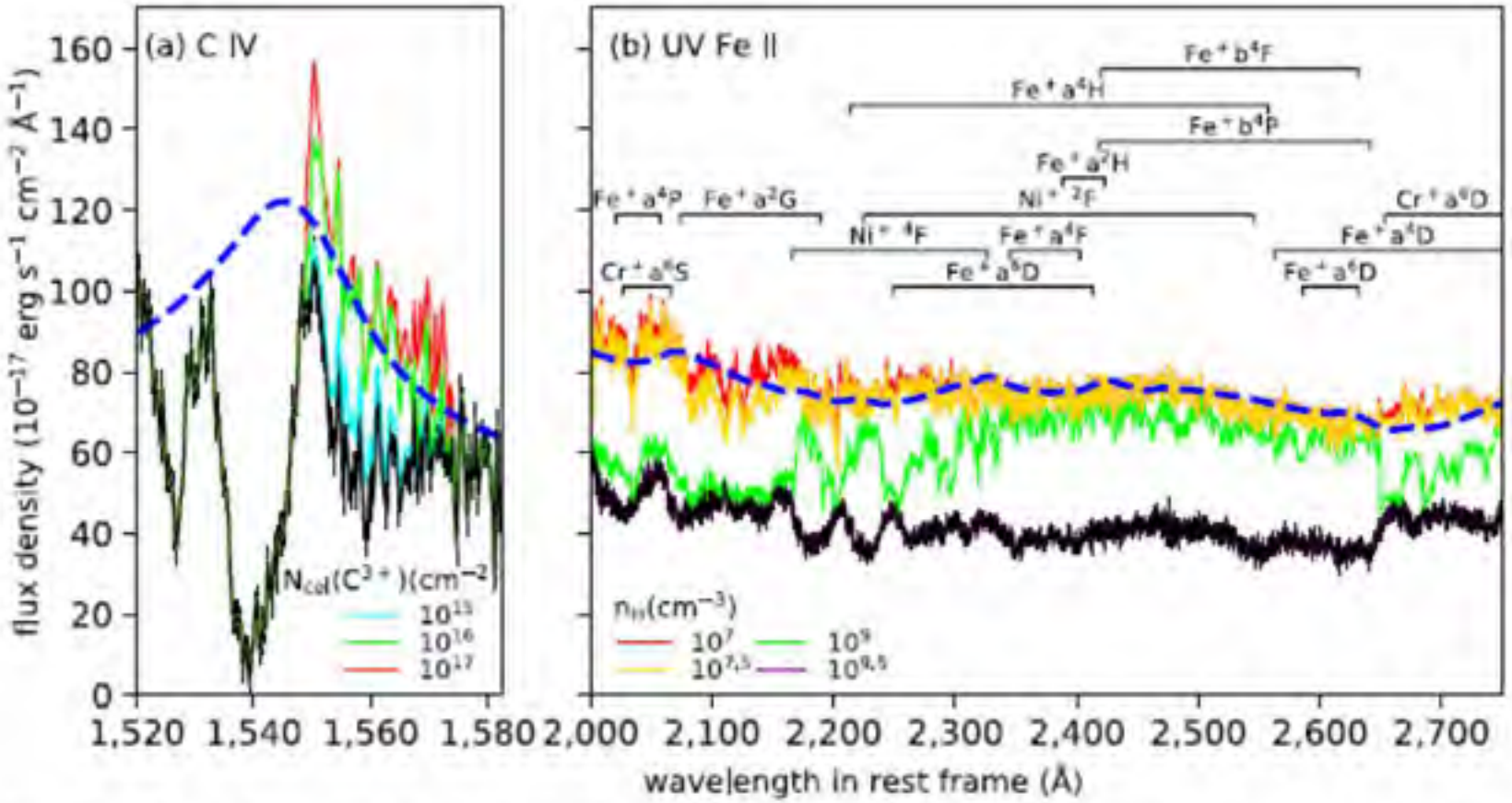

Extended Data Fig. 6 | Comparison between observation and model calculations for selected metal absorption lines. a, Recovered spectra of C IV, corrected for redshifted absorption, assuming C^{3+} ion column densities of $N_{col}(C^{3+}_{ground}) = 10^{15}$, 10^{16} and 10^{17} cm^{-2} in the quasar's rest frame. The error bars on the observed flux denote 1σ uncertainty. Compared with the best-fit SDSS composite spectrum (blue dashed line), the recovered flux is much too weak for the absorption when $N_{col}(C^{3+}_{ground}) = 10^{15}$ cm^{-2}, while it is too high (showing two extra deceptive peaks at around 1,550 and 1,570 Å) for the absorption when $N_{col}(C^{3+}_{ground}) = 10^{17}$ cm^{-2}. The absorption model with $N_{col}(C^{3+}_{ground}) \approx 10^{16}$ cm^{-2} predicts unabsorbed flux that is reasonably consistent with the composite spectrum, and is thus adopted. **b**, Absorption-corrected UV Fe II spectra between 2,000 and 2,750 Å for the post-C^{3+} inflow models with $n_H = 10^7$ cm^{-3} (red), $10^{7.5}$ cm^{-3} (yellow), 10^8 cm^{-3} (green), and $10^{8.5}$ cm^{-3} (violet) in the high 'probability' zone of Extended Data Fig. 5b. The error bars on observed flux are 1σ uncertainties. Compared with the best-fit composite (blue dashed line), the models with higher densities can be clearly ruled out.

distance constrained by photoionization models of HI* and HeI*

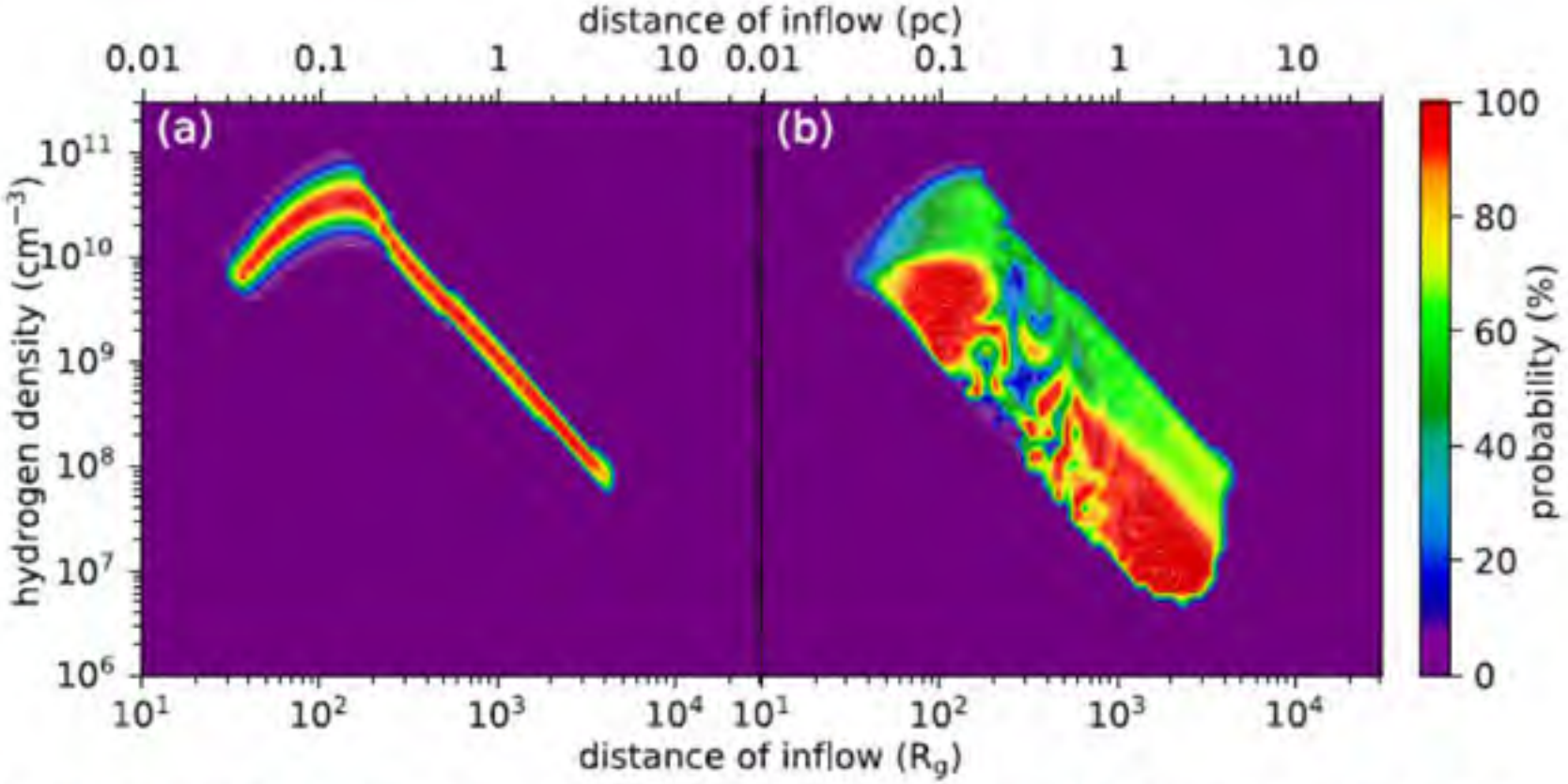

Extended Data Fig. 5 | Probability density distribution in the parameter space of the total hydrogen density (n_H) and distance from the central engine (d_{inflow}) for different inflow models. a, The simplest primordial models are applied, and the redshifted H I* and He I* broad absorption lines are used to evaluate the probability density. However, the highly probable models predict much higher column densities of C^{3+} ions ($N_{col}(C^{3+}_{ground})$) than that estimated from the redshifted C IV broad-absorption-line trough. **b**, To resolve this problem, only the region beyond the C^{3+} region (the 'post-C^{3+} region') in the primordial models is used to describe the inflow gas, and probability density is recalculated by including C IV. The results of these refined model calculations are shown here. The probability density shows two peaks around $n_H \approx 10^7$ cm^{-3} and $d_{inflow} \approx 2{,}000R_g$, and $n_H \approx 10^{8.5}$ cm^{-3} and $d_{inflow} \approx 100R_g$ (see also Fig. 3).

distance by HI, HeI* and metal BALs

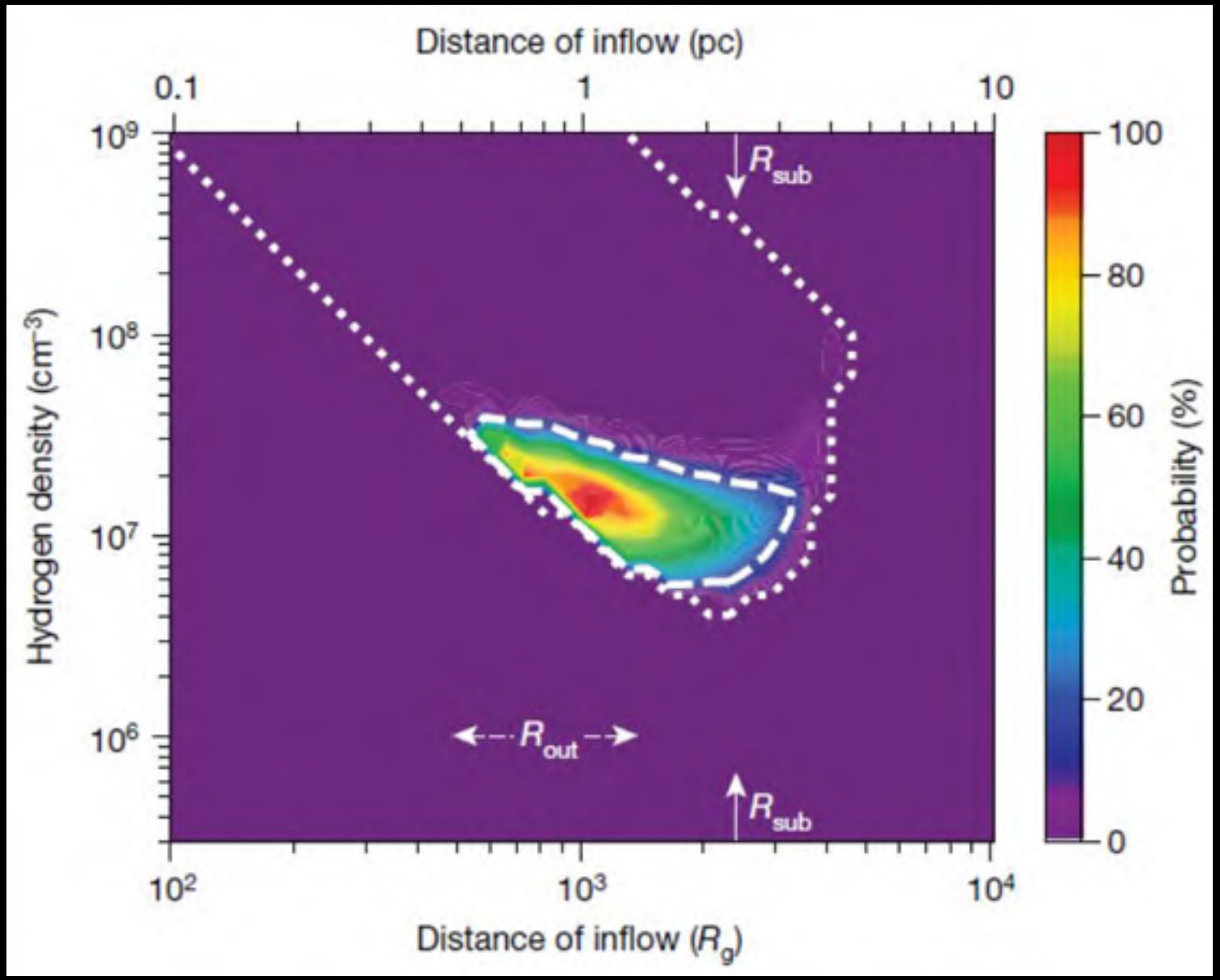


LETTER

Fast inflows as the adjacent fuel of supermassive black hole accretion disks in quasars

“the last piece of the puzzle falls in place”

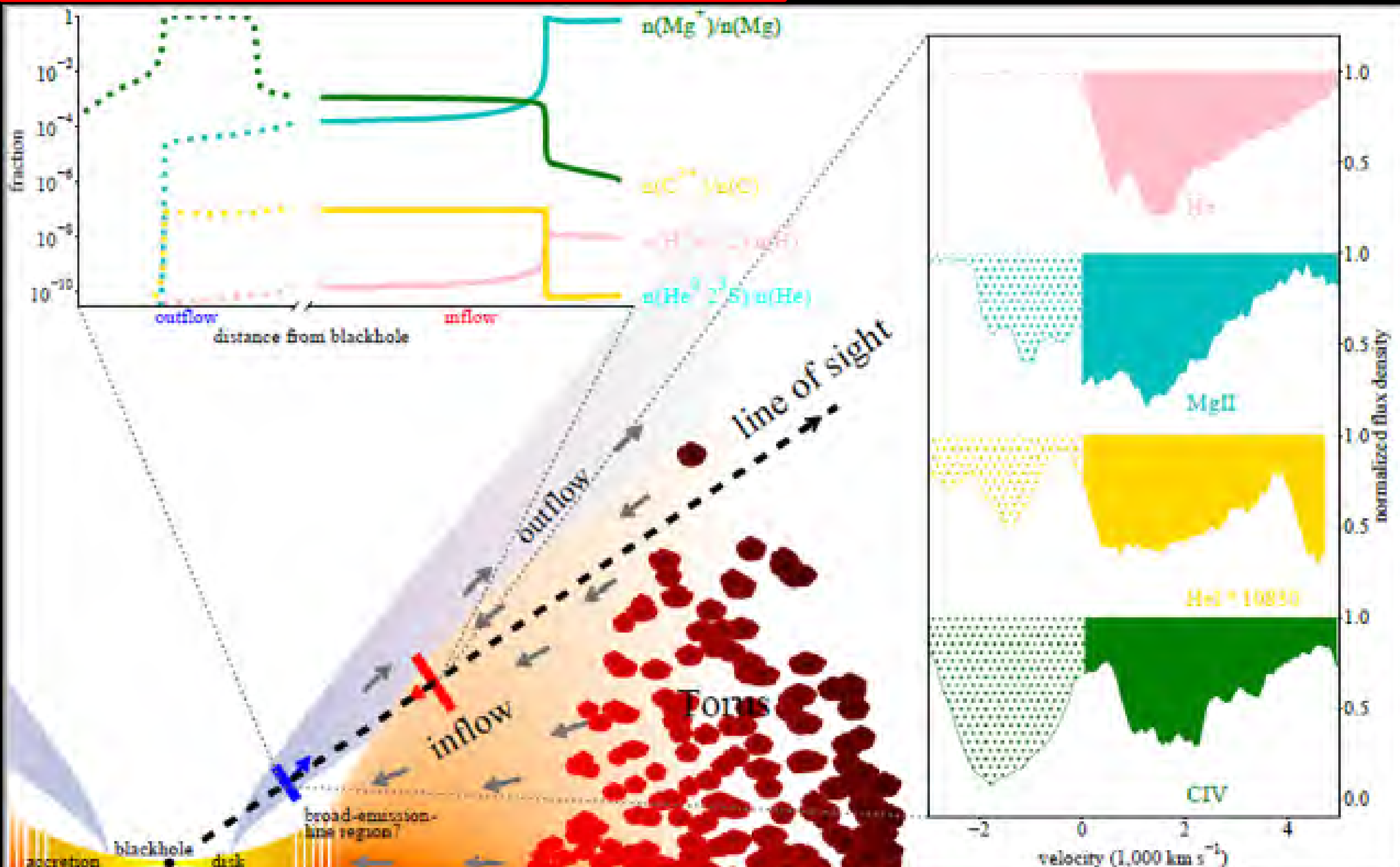

AA Tauri（“金牛”, V = $0^m.8$)

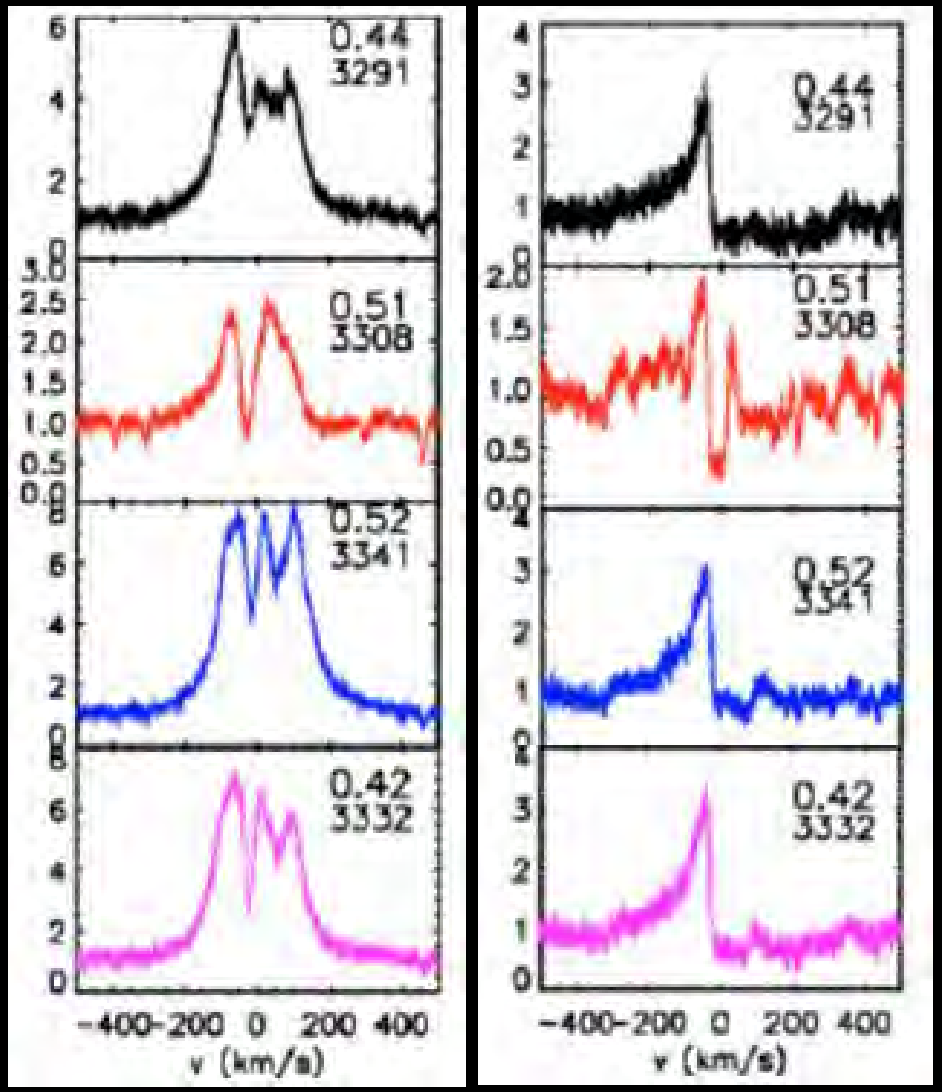

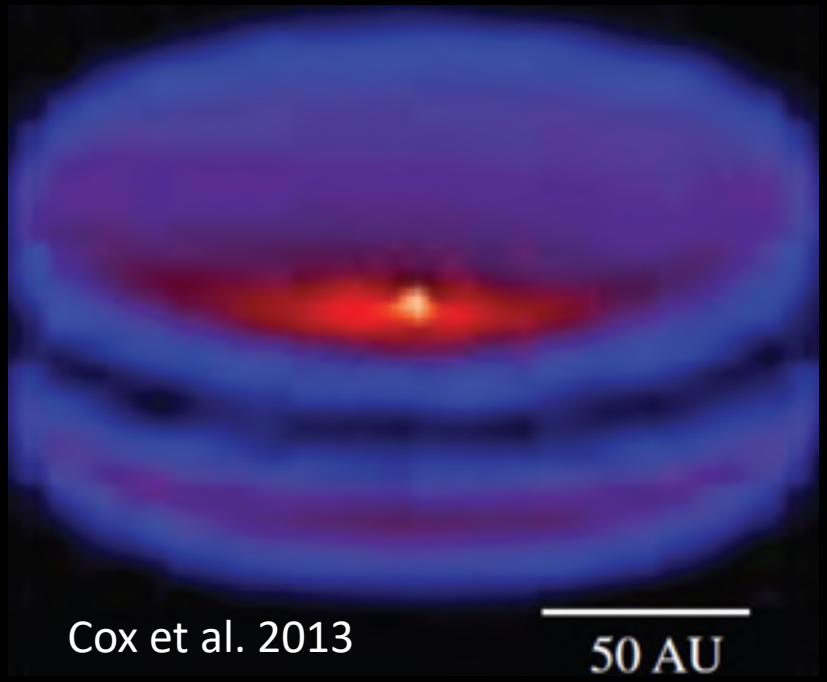

Cox et al. 2013

accretion from the circumstellar disk (or occultation of the star by material in the disk) revealed by **redshifted Hα and Hβ** absorption lines.

Bouvier et al. 2007, A&A 463, 1017–1028

ionization structure and metallicities

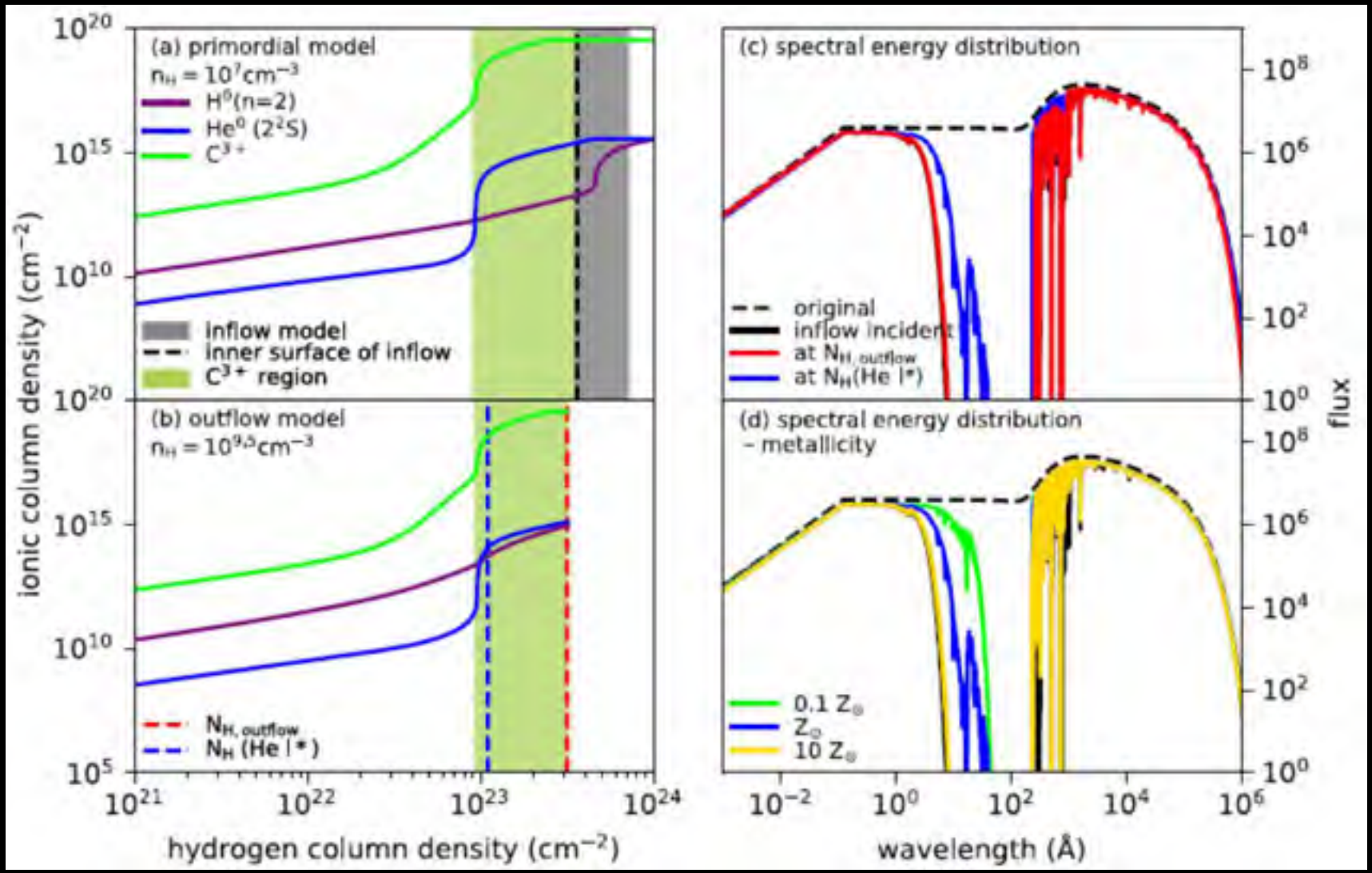

5. J1035+1422's analogues

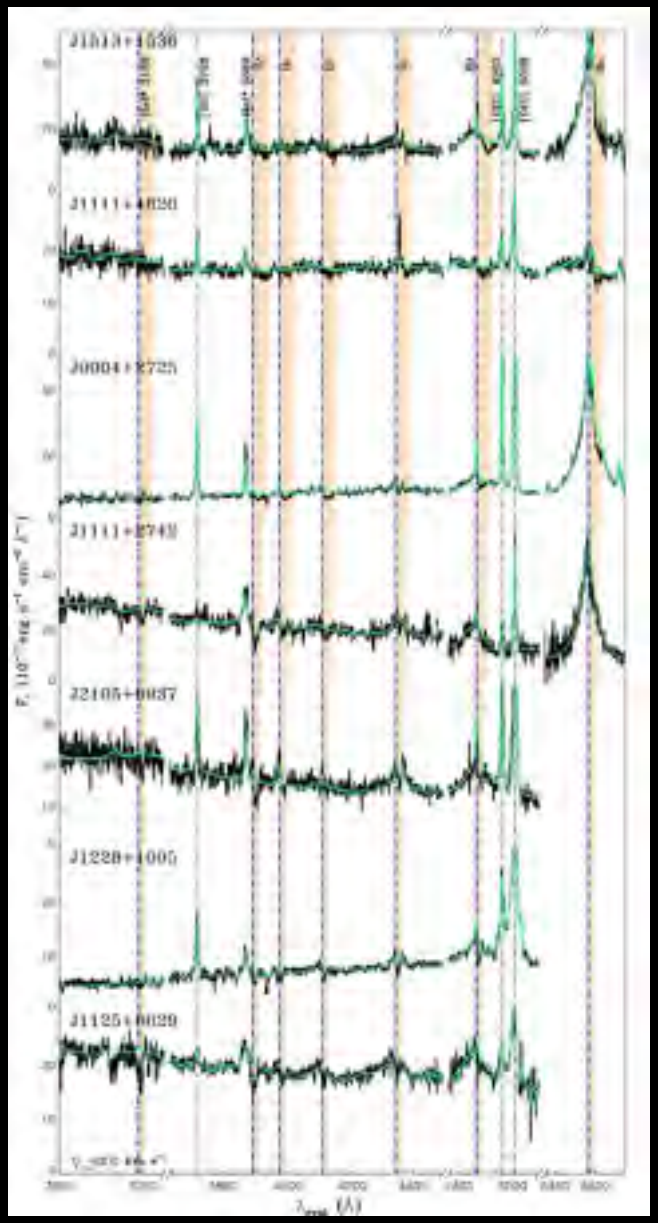

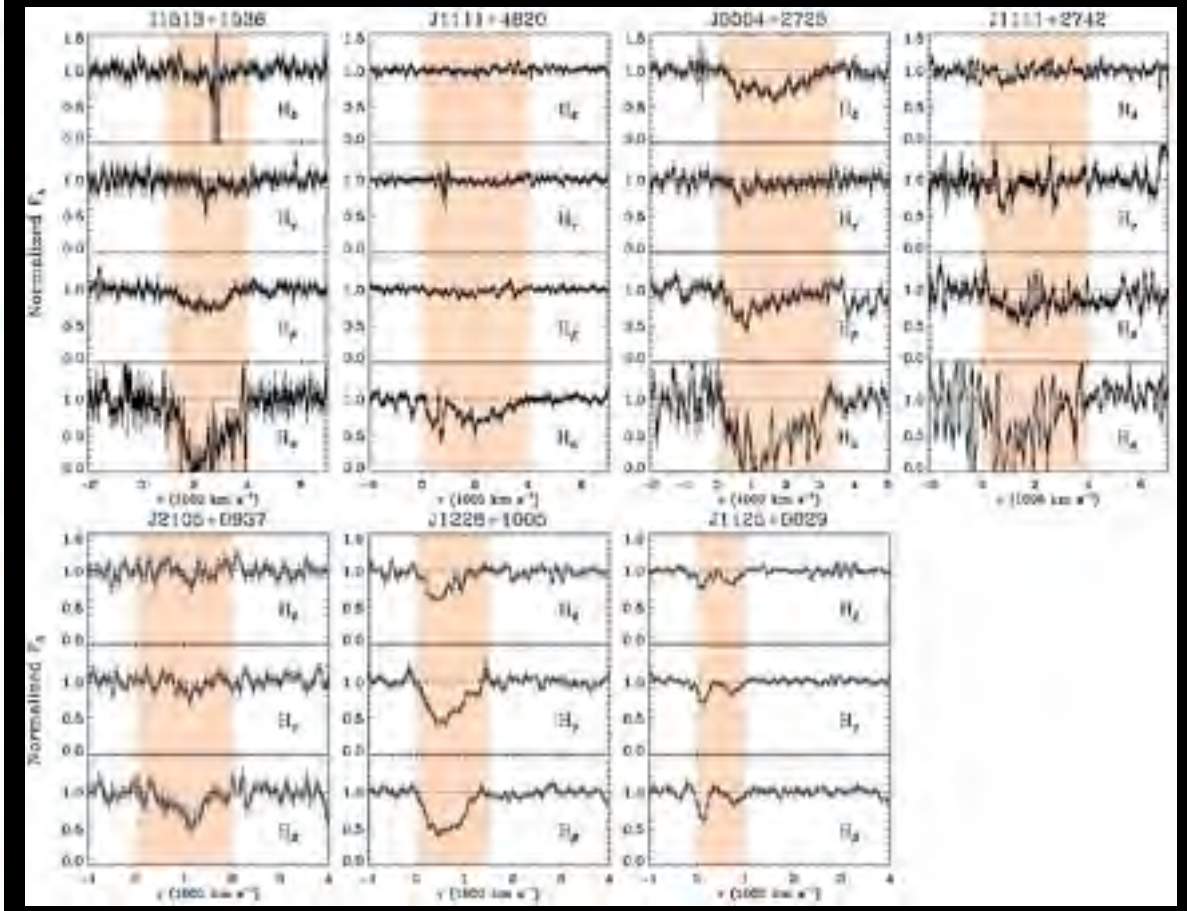

5. the last piece of the puzzle?

- *ISM inflows → galactic nuclear region （headstream✔？ ）*
- **disk feeding inflows（DFI ✔）**
- *disk inflows （end ✔ ？ ）*

black hole accretion disks:

imagination is beautiful, reality is skeletal ?

Credit: NASA, Jeremy Schnittman

curtain remains open: NGC 2617

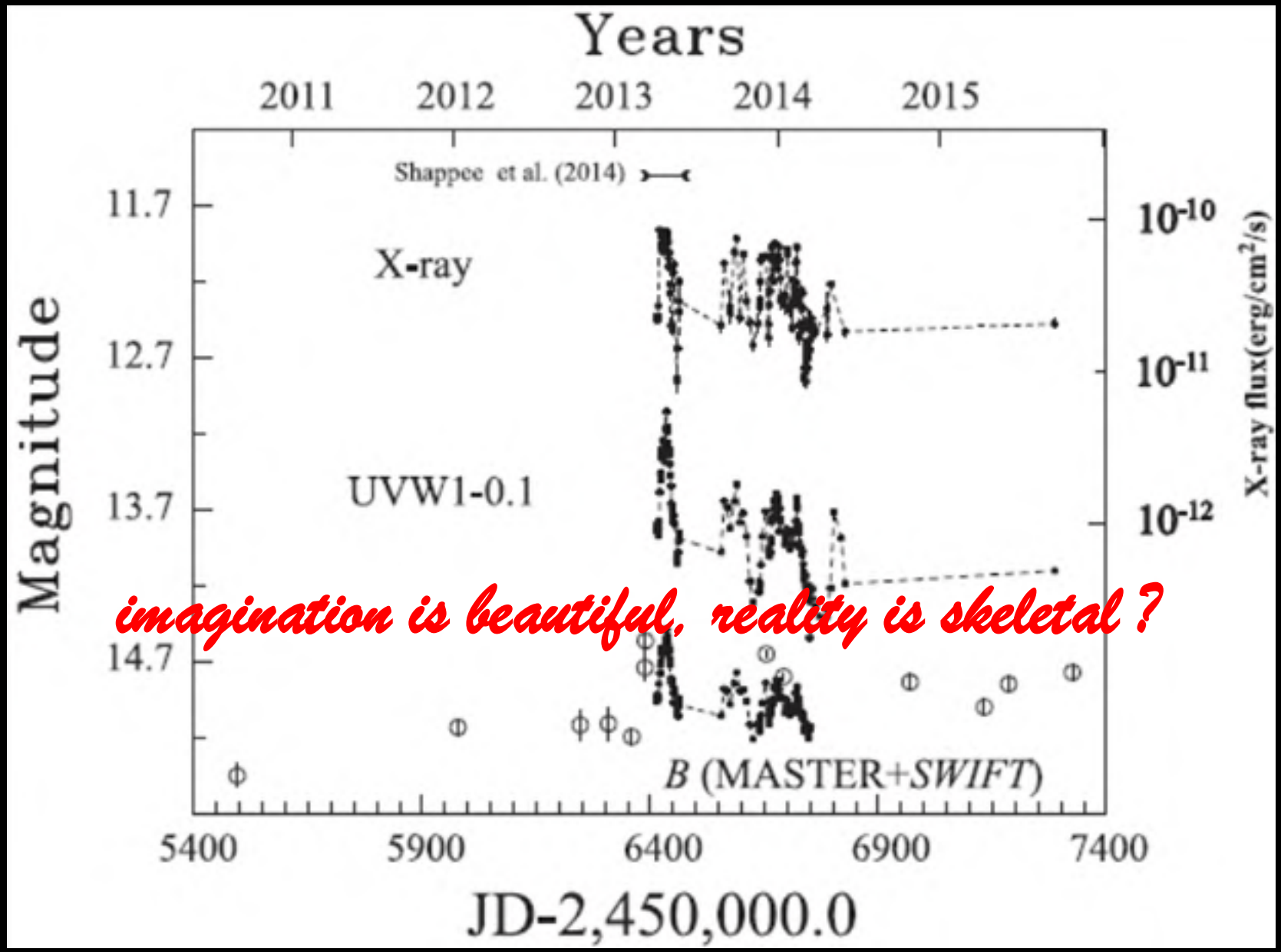

imagination is beautiful, reality is skeletal ?

Probing the Accretion Disk-Feeding Inflow for a Unique Redshift-BAL AGN Sample

PI: C. Jin, CoI: H. Zhou, W. Yuan, P. Jiang, X. Pan, X. Shi

1. Abstract

A fundamental question remains unanswered about AGN is how the accretion disc is fed with external gas. Recently, Zhou et al. (2019) present the first compelling evidence for the long-sought inflow directly feeding the disc, and propose a global scenario including both inflow and outflow. However, there is still a lack of crucial knowledges from the X-ray band. Here we propose 6 carefully selected sources from Zhou et al.'s redshift-BAL AGN sample for *XMM-Newton* observations, including a superb archetypal source for a deep exposure. This program will provide valuable X-ray data for investigating various X-ray absorption features in these AGN, verifying their disc-feeding inflow scenario, and exploring detailed properties of the inflow and outflow materials, thereby allowing us to better understand the AGN fuelling mechanism.

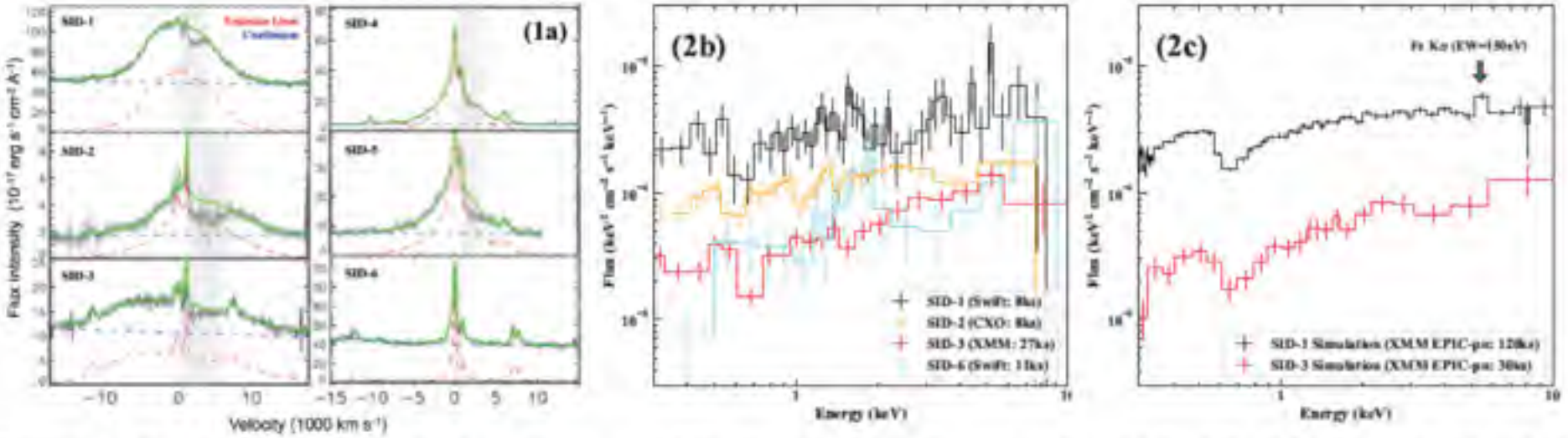

Figure 2: Panel-a: fitting the optical spectrum around Hα line for all the 6 sources. A redshifted Hα-BAL is clearly identified in every sources as indicated the gray region. Panel-b: the X-ray spectra of 4 sources from archival observations, where the signature of OVII K absorption edge can be seen at ~0.6 keV (AGN rest-frame). Panel-c: the simulated *XMM-Newton* EPIC-pn spectra for 120 ks of SID-1 and 30 ks of SID-3 to demonstrate the spectral quality that is required by our research objectives.

previous detections in the X-rays

CXOC J100043.1+020637 Civano et al. 2010).

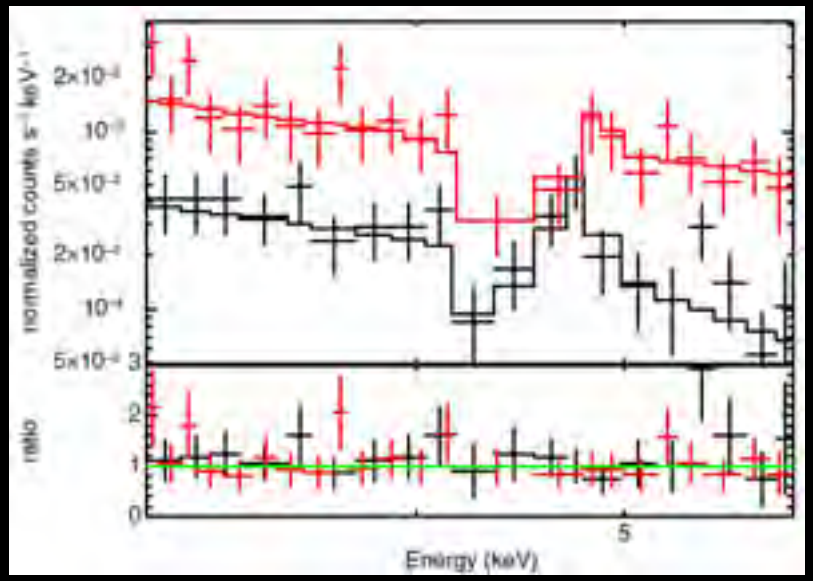

NGC 2617 (Giustini et al. 2018)

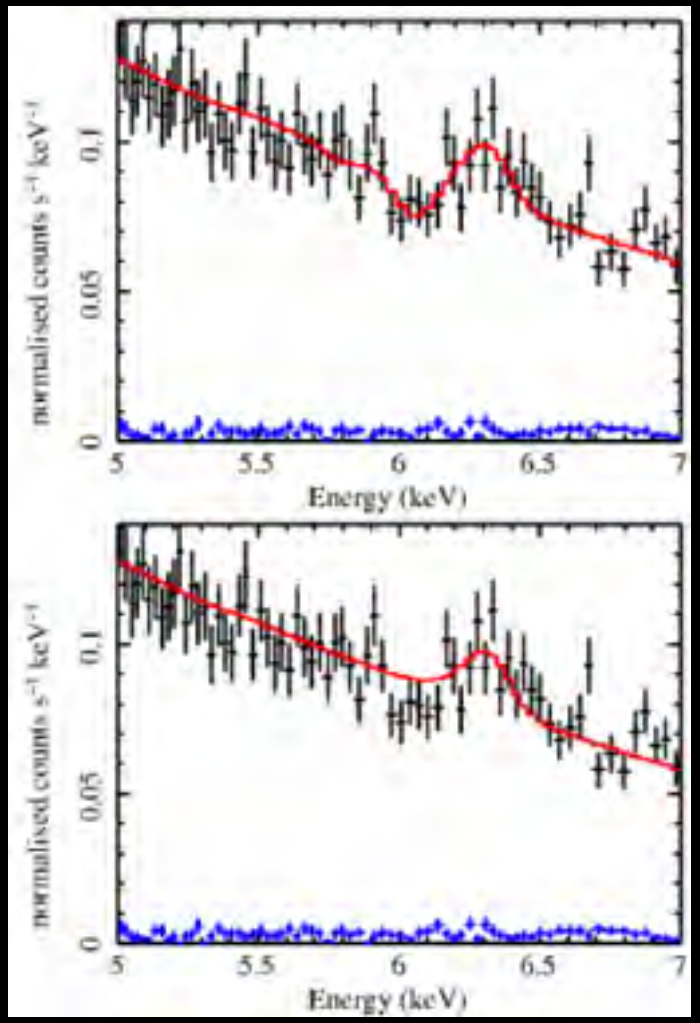

The redshifted absorber can be ascribed to a **failed wind/aborted jets component**, to **gravitational redshift** effects, and/or to **matter directly falling towards the central supermassive black hole**.

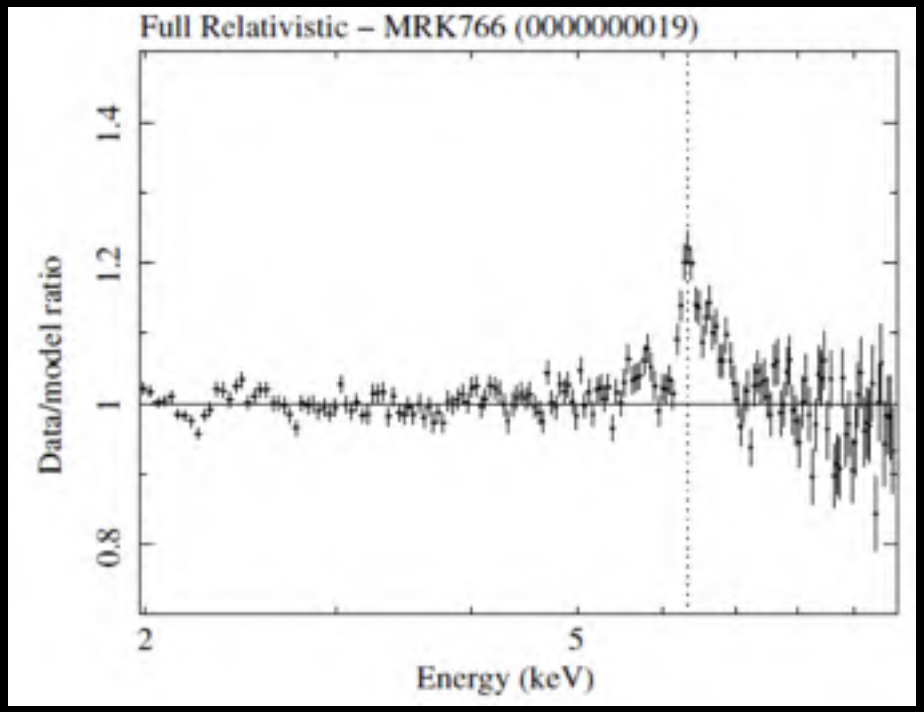
Full Relativistic – MRK766 (0000000019)
Data/model ratio
0.8
1
1.2
1.4
2
5
Energy (keV)

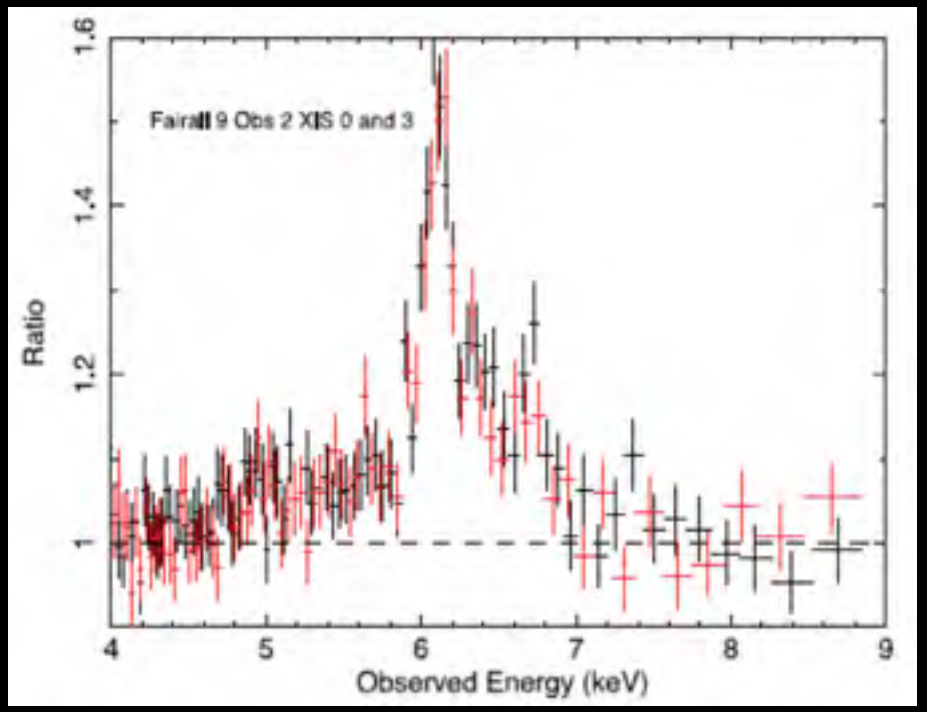
Fairall 9 Obs 2 XIS 0 and 3
Ratio
1
1.2
1.4
1.6
4
5
6
7
8
9
Observed Energy (keV)

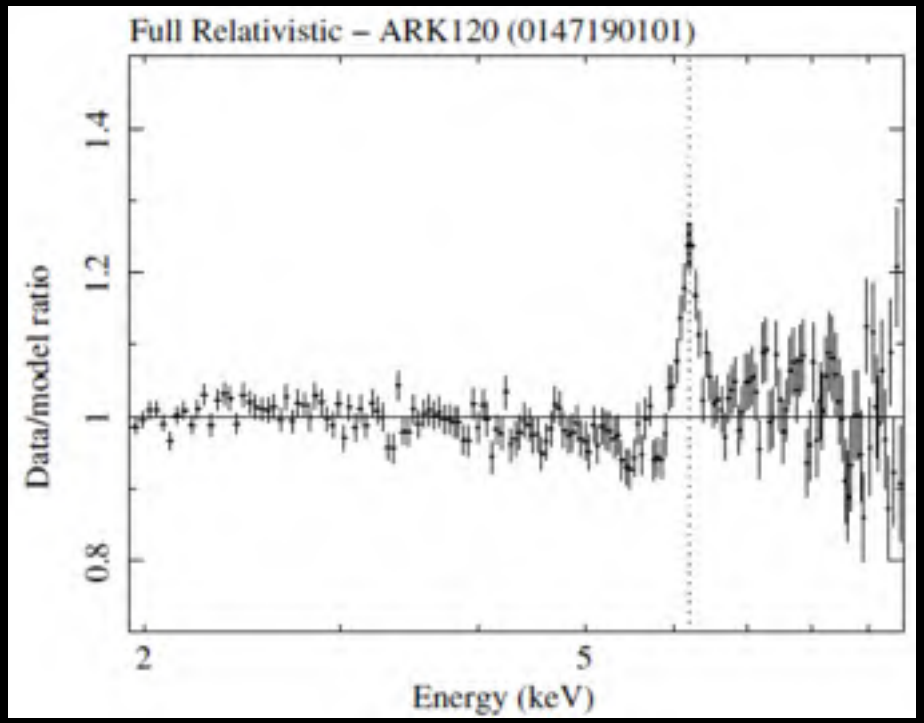
Full Relativistic – ARK120 (0147190101)
Data/model ratio
0.8
1
1.2
1.4
2
5
Energy (keV)

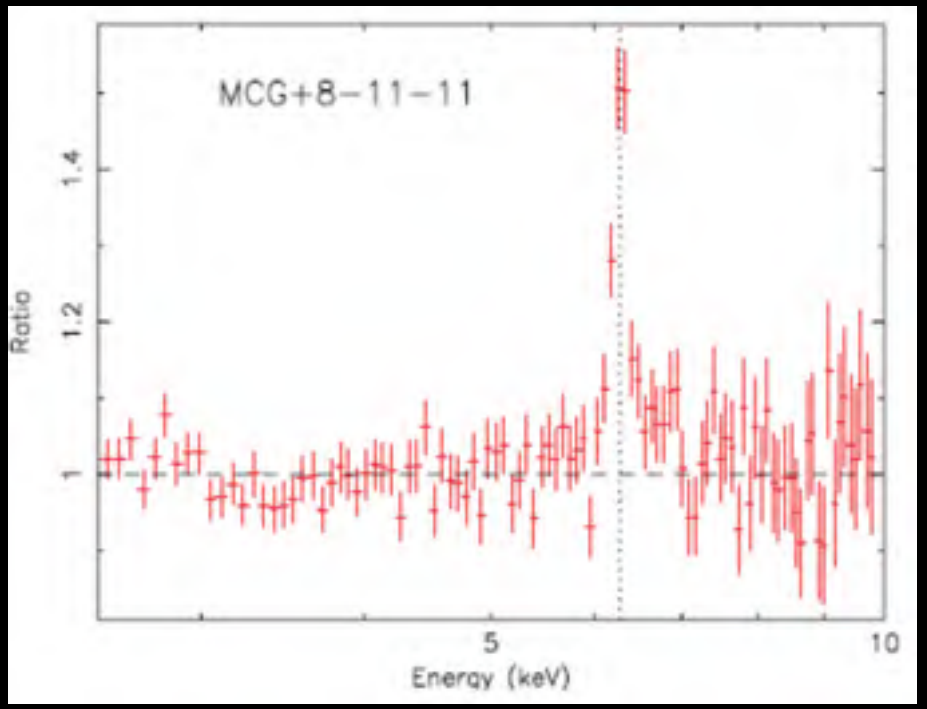
MCG+8−11−11
Ratio
1
1.2
1.4
5
10
Energy (keV)

the end of BH accretion flows (EP)

headstream (✔?) of accretion flows in the radio

A hyperfine transition exists for hydrogen atoms in the ground state $1\ ^2S_{1/2}$: Depending on the relative spins of the proton and the electron, there is a very small difference in the energy of the ground state $\Delta E = 5.87\ \mu eV \sim 1.4\ GHz \sim \mathbf{21\ cm}$.

$$\frac{n_u}{n_l} = \frac{g_u}{g_l} exp\left(-\frac{h\nu}{k_B T_s}\right) \approx \frac{3}{1};$$

$$T_B(v) = C_f T_C e^{-\tau(v)} + \left[1 - C_f\right]T_c + \left[1 - e^{-\tau(v)}\right];$$
$$\Delta T(v) = T_B(v) - T_C = \left[T_s - C_f T_C\right]\left[1 - e^{-\tau(v)}\right].$$

Line emission ($T_s - C_f T_C$>0):

$$T_B(v) \approx \tau(v) T_s \propto \frac{N_{HI}}{T_s} T_s;$$

$$N_{HI} = 1.82 \times 10^{18}[cm^{-2}] \int T_B(V)\,[K] dV [km \cdot s^{-1}].$$

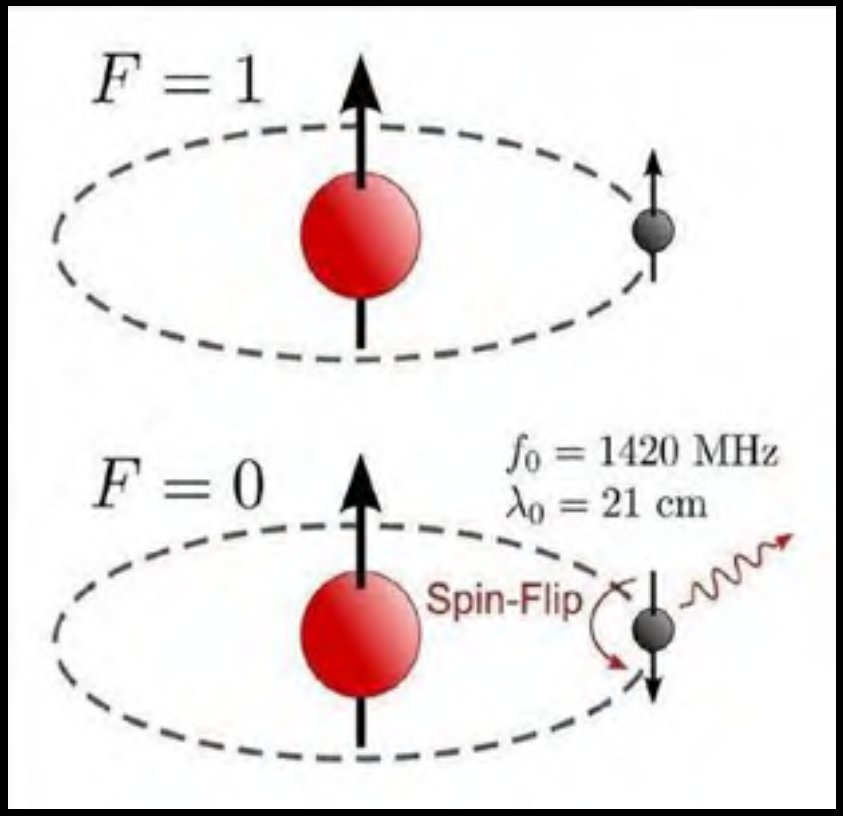

Line absorption ($T_s - C_f T_C < 0, \tau \ll 1$):

$$N_{HI} = 1.82 \times 10^{18}[cm^{-2}] \frac{T_s}{C_f T_C} \int \Delta T(V)\,[K] dV [km \cdot s^{-1}] \text{ (for } \tau \ll 1).$$

headstream in the radio ✔(?)

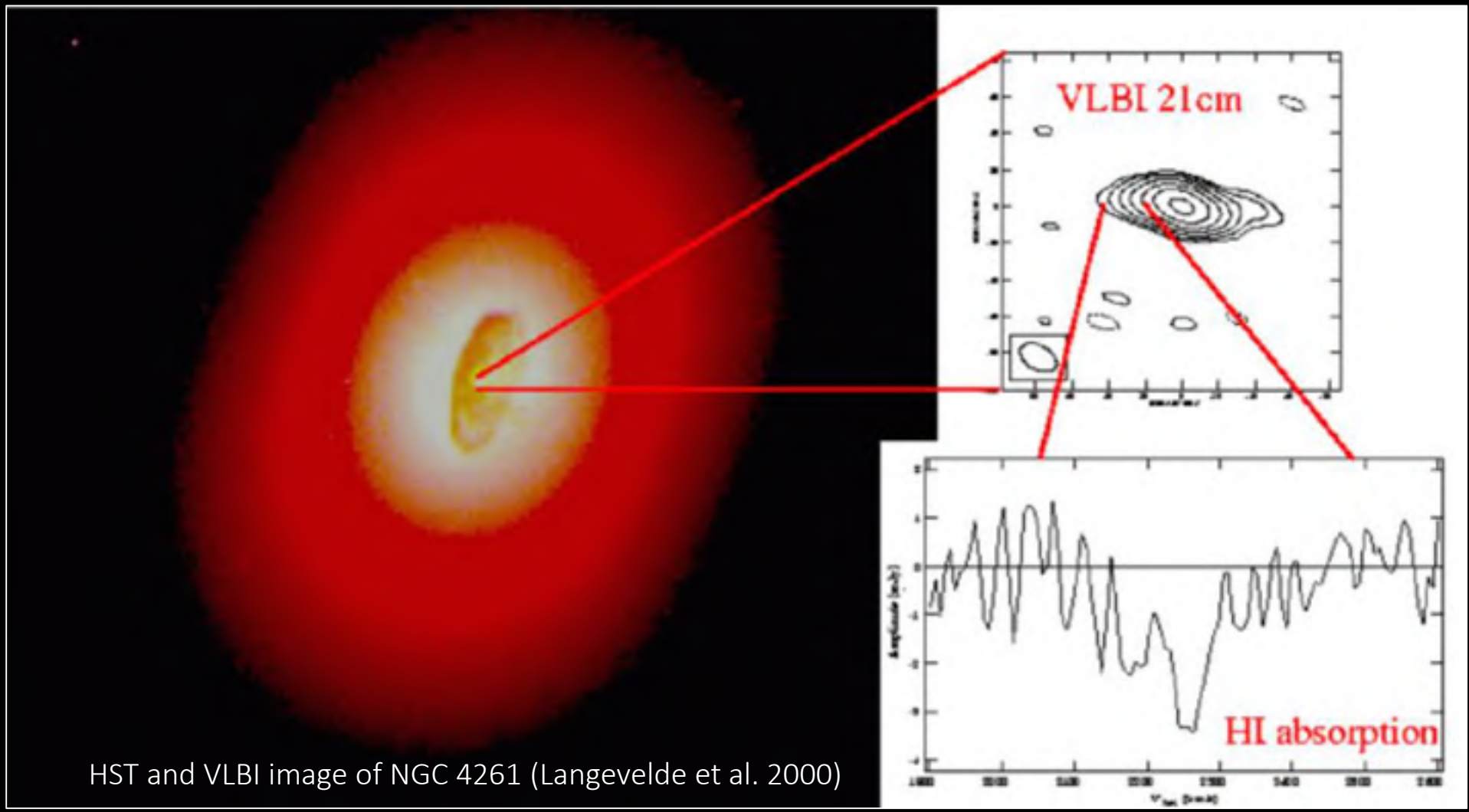

HST and VLBI image of NGC 4261 (Langevelde et al. 2000)

headstream in the radio ✔(?)

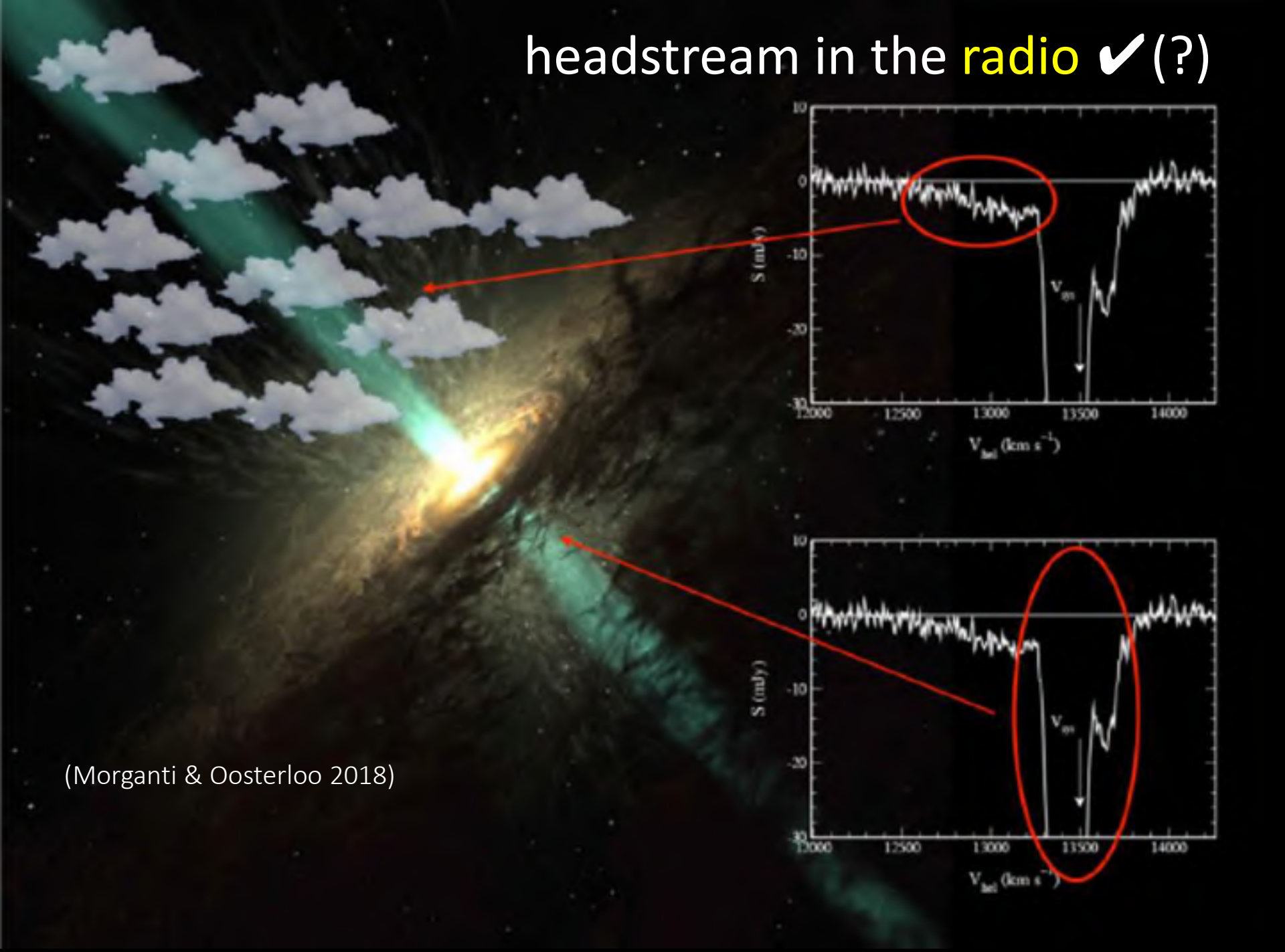

(Morganti & Oosterloo 2018)

headstream in the infrared ✔(?)

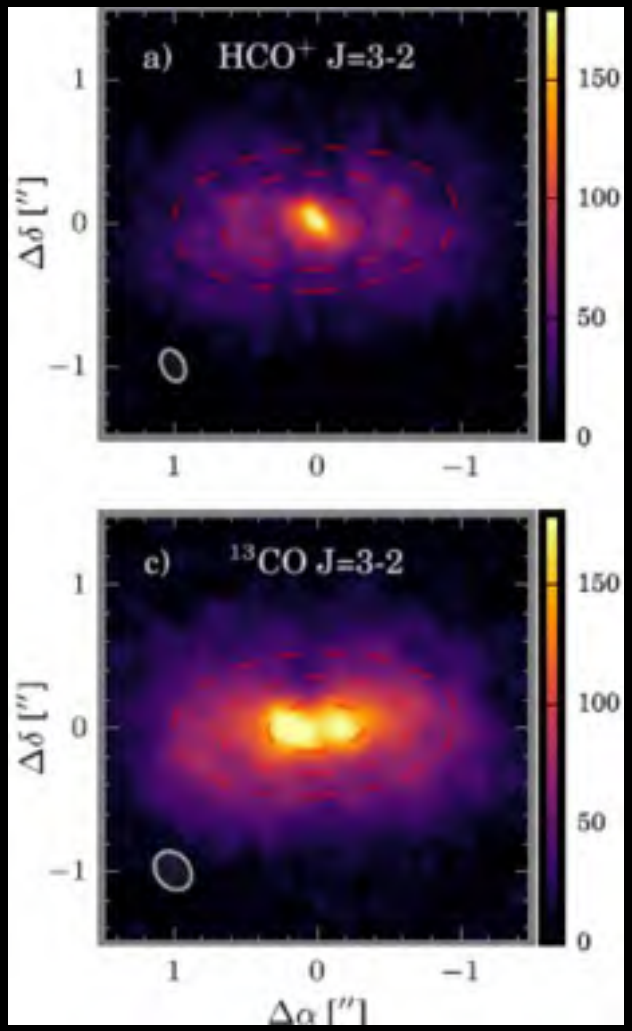

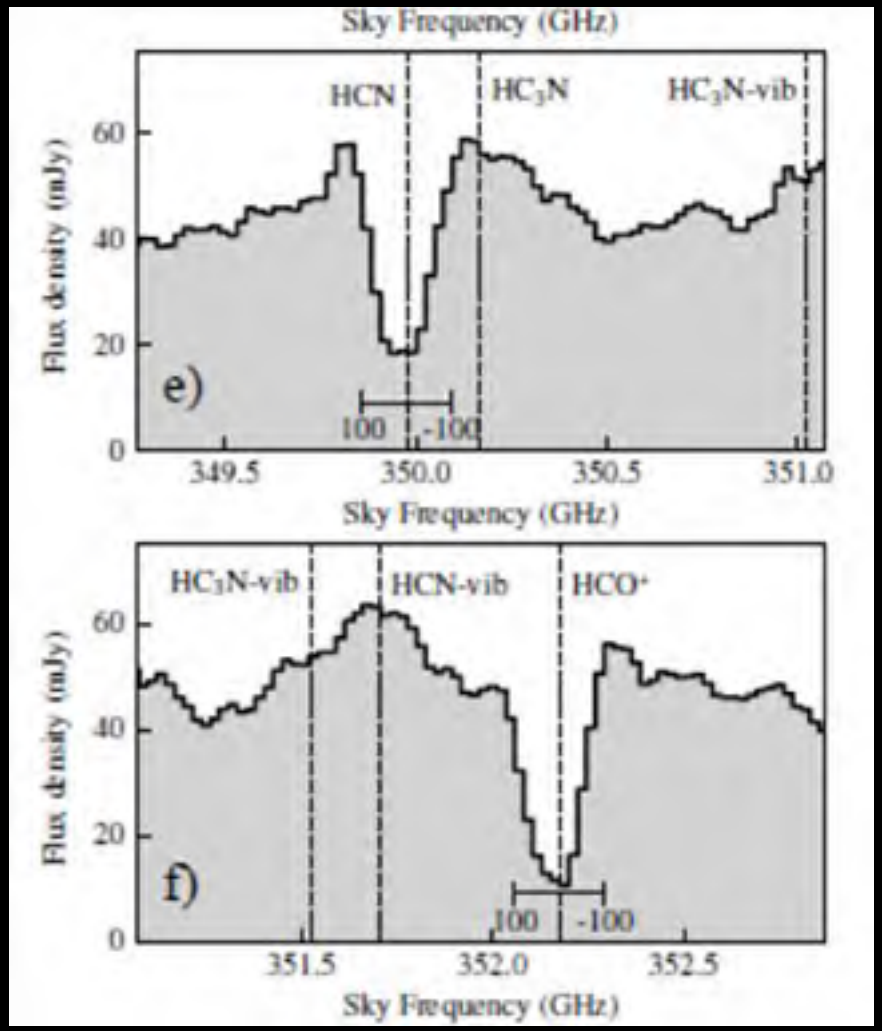

Aalto et al. 2019

model & observation of stellar mass black holes

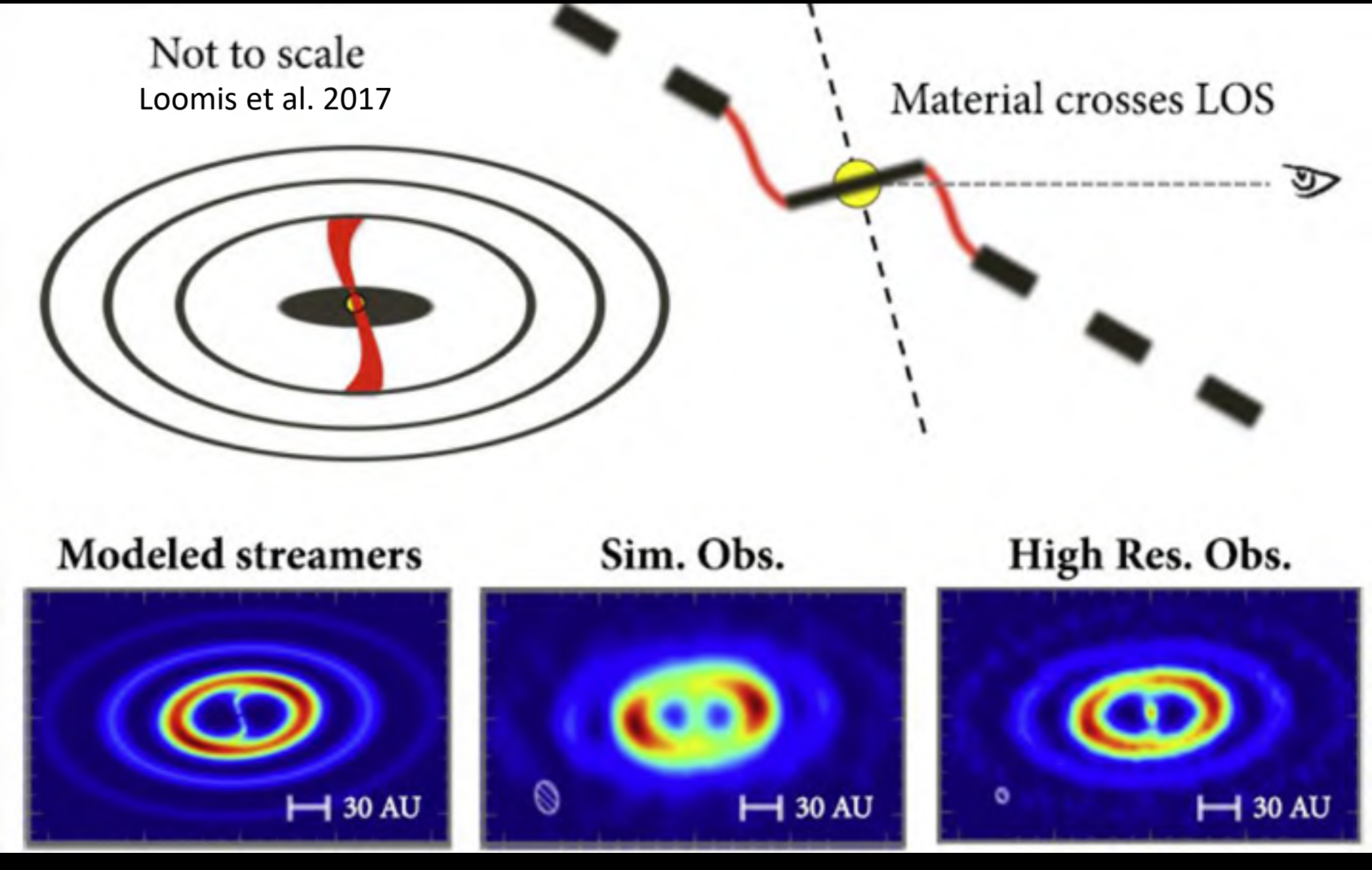

theories & observations of accretion flows

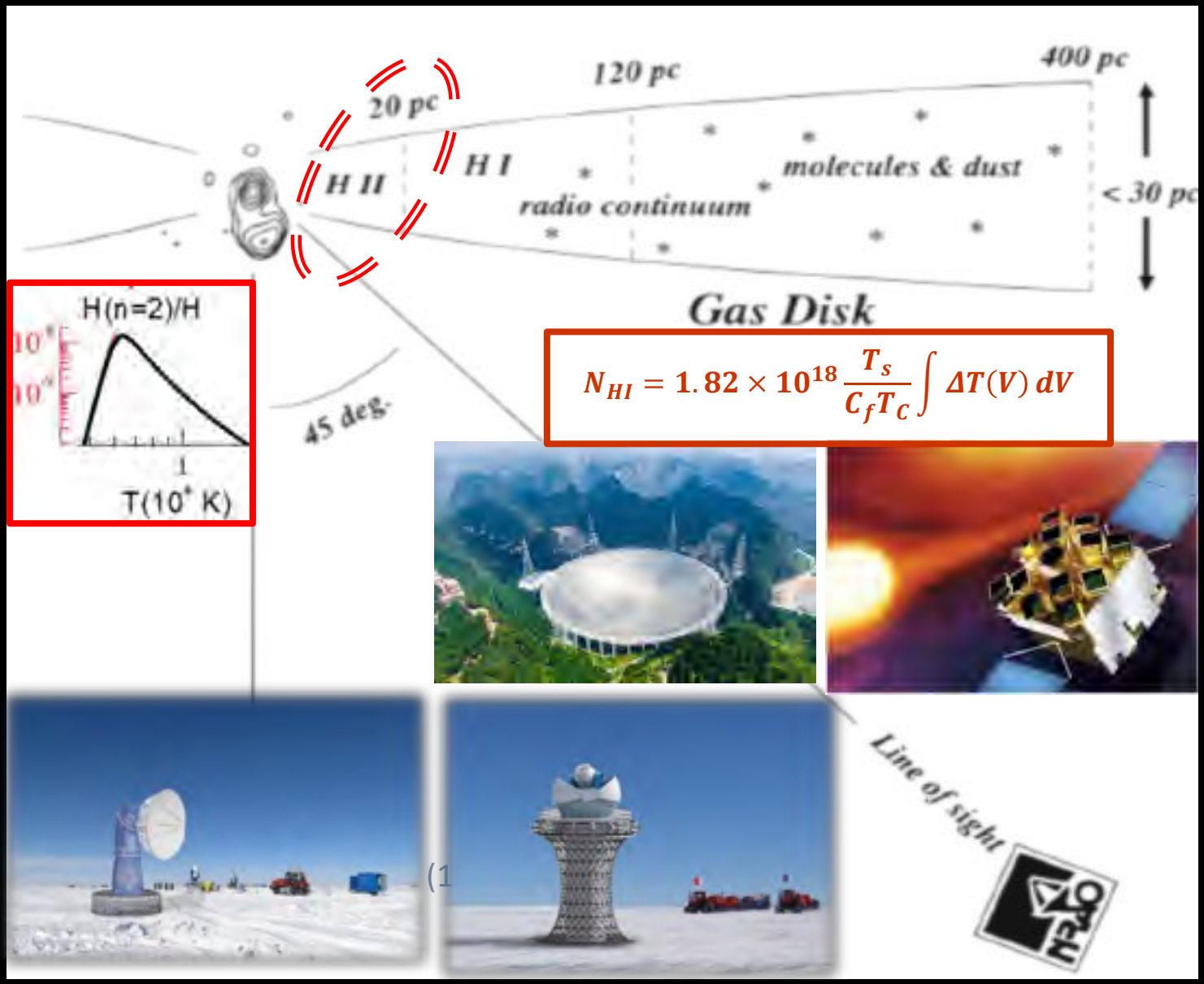

叶叔华院士寄语

2020年6月29日

我觉得南极天文台，不但是国家的一个重要基地，而且是各方面应用都可以使用的，而且它已经有很多年的基础，可以自动控制、自动传输，经验还是很丰富的。飞过两极的卫星非常多，其中有很多都是侦察卫星、军用卫星。除此之外，这个地点还可以作为以后的远程测控的一个基地。比方，我们飞到以后的深空探测，如果需要的话，这是唯一可用的一个最南端的观测点。所以我非常希望保留这个观测点，并且随着国家的应用加以发挥。

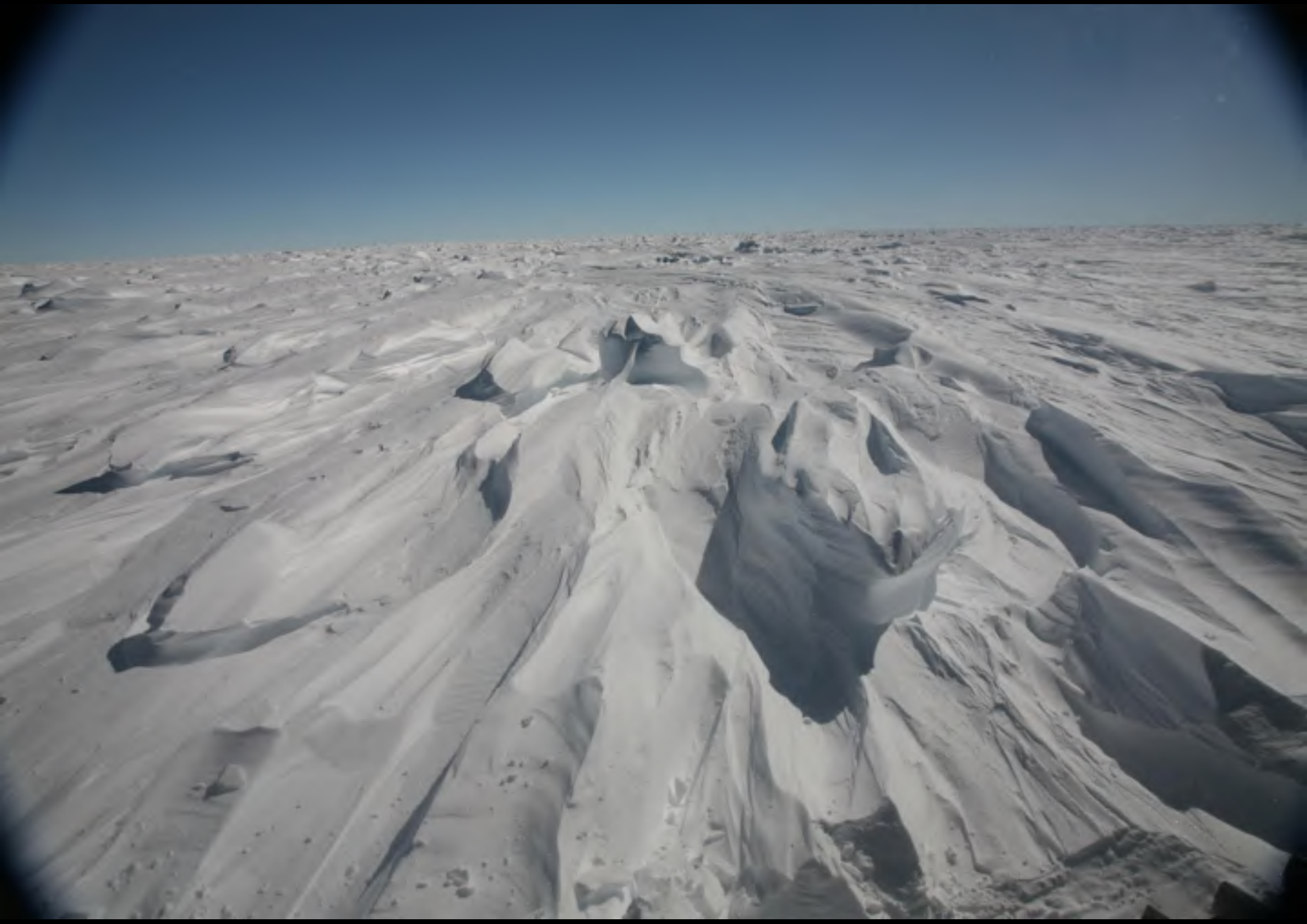


CATERPILLAR
29th CHINARE
1223新选站址

海上升明月，天涯共此时

6. What next

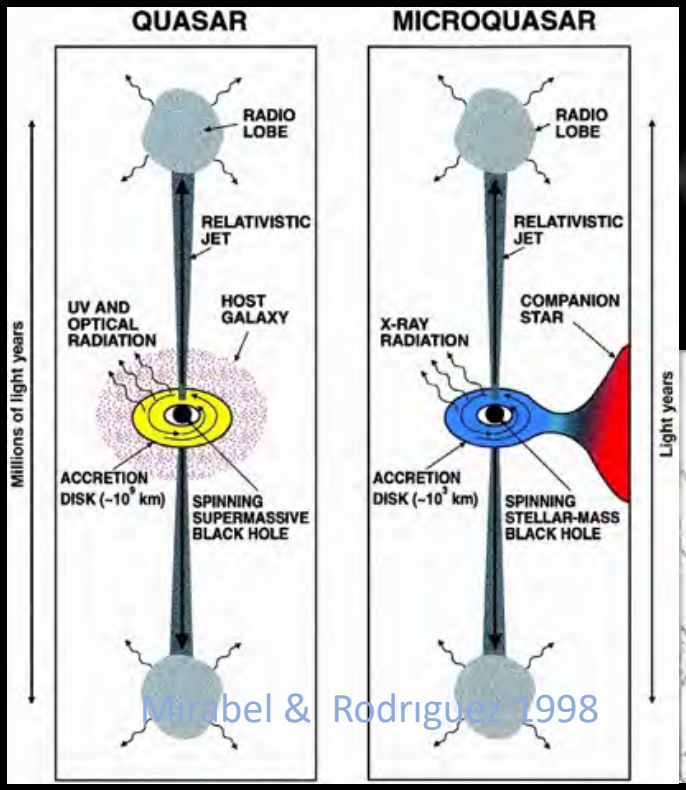

Mirabel & Rodriguez 1998

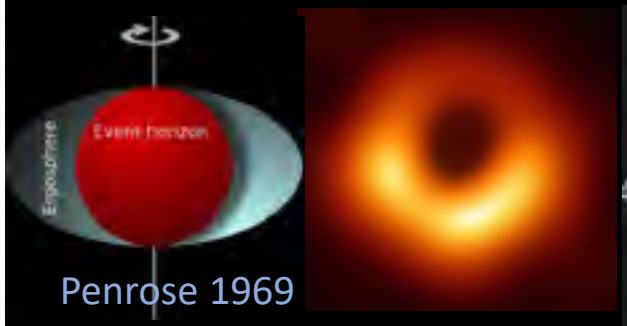

Penrose 1969

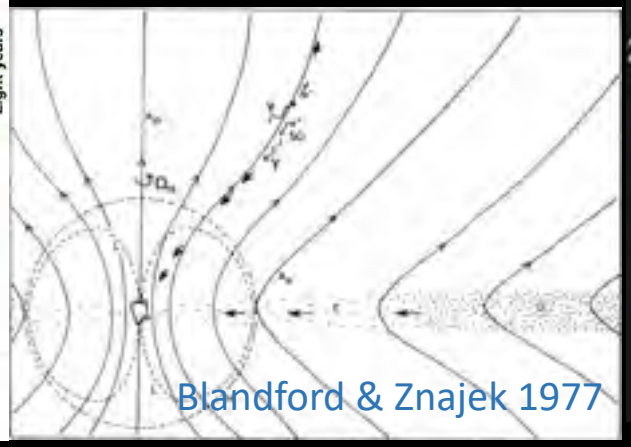

Blandford & Znajek 1977

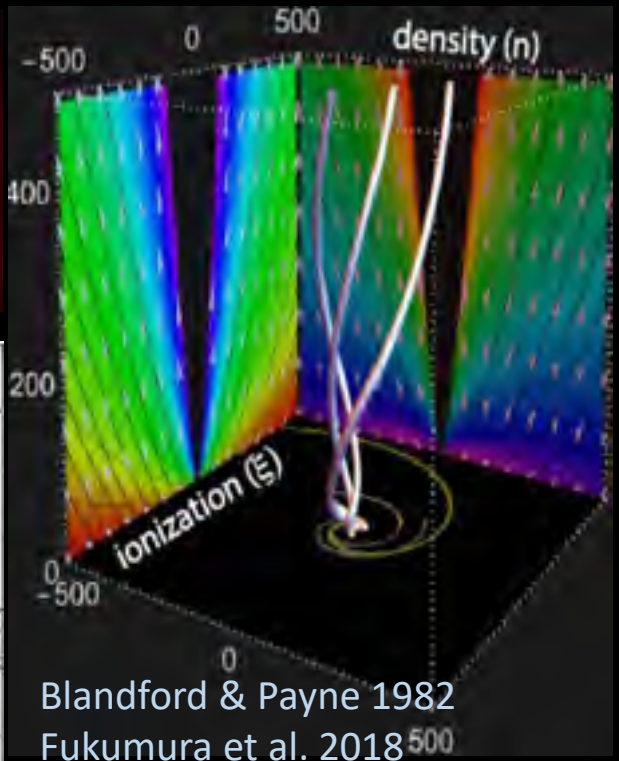

Blandford & Payne 1982
Fukumura et al. 2018

天文学重大突破正在加速

1960-2010，每5-10年获得1次诺贝尔物理学奖

2011-2019，每2-3年获得1次诺贝尔物理学奖

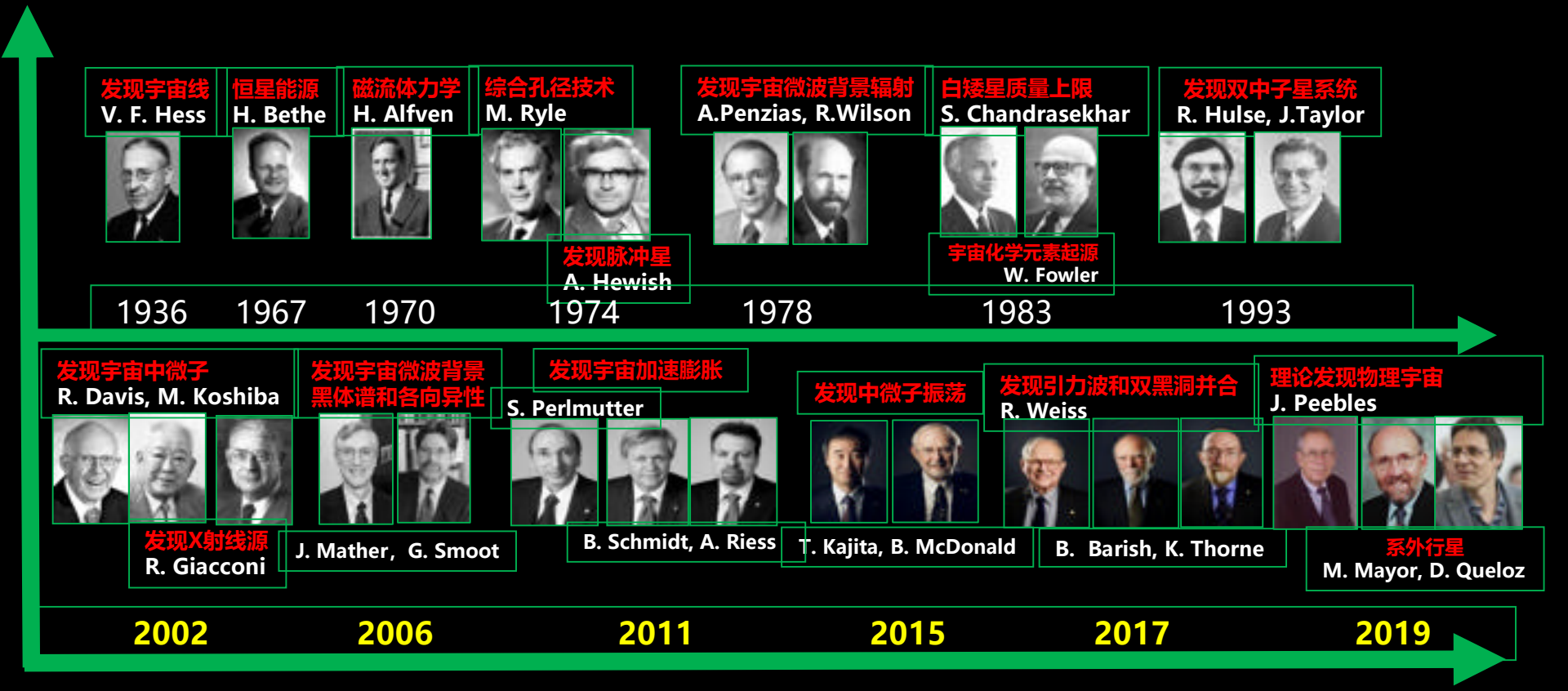

- 习近平(2012)：“空间天文和南极天文等重要前沿研究领域取得重要进展”